Space Sci Rev (2011) 163:141–174
DOI 10.1007/s11214-010-9637-z

HED Meteorites and Their Relationship to the Geology of Vesta and the Dawn Mission

Harry Y. McSween Jr. · David W. Mittlefehldt · Andrew W. Beck · Rhiannon G. Mayne · Timothy J. McCoy

Received: 25 September 2009 / Accepted: 11 February 2010 / Published online: 17 March 2010

Abstract Howardite-eucrite-diogenite (HED) meteorites, thought to be derived from 4 Vesta, provide the best sampling available for any differentiated asteroid. However, deviations in oxygen isotopic composition from a common mass-fractionation line suggest that a few eucrite-like meteorites are from other bodies, or that Vesta was not completely homogenized during differentiation. The petrology and geochemistry of HEDs provide insights into igneous processes that produced a crust composed of basalts, gabbros, and ultramafic cumulate rocks. Although most HED magmas were fractionated, it is unresolved whether some eucrites may have been primary melts. The geochemistry of HEDs indicates that bulk Vesta is depleted in volatile elements and is relatively reduced, but has chondritic refractory element abundances. The compositions of HEDs may favor a magma ocean model, but inconsistencies remain. Geochronology indicates that Vesta accreted and differentiated within the first several million years of solar system history, that magmatism continued over a span of ~ 10 Myr, and that its thermal history extended for perhaps 100 Myr. The protracted cooling history is probably responsible for thermal metamorphism of most HEDs. Impact chronology indicates that Vesta experienced many significant collisions, including during the late heavy bombardment. The age of the huge south pole crater is controversial, but it probably ejected Vestoids and many HEDs. Continued impacts produced a regolith composed of eucrite and diogenite fragments containing only minor exotic materials. HED meteorites serve as ground truth for orbital spectroscopic and chemical analyses by the Dawn spacecraft, and

H.Y. McSween Jr. (✉) · A.W. Beck
Planetary Geoscience Institute and Department of Earth & Planetary Sciences, University of Tennessee, Knoxville, TN 37996-1410, USA
e-mail: mcsween@utk.edu

D.W. Mittlefehldt
Astromaterials Research Office, NASA Johnson Space Center, Houston, TX 77058, USA

R.G. Mayne
Department of Geology, Texas Christian University, TCU Box 298830, Fort Worth, TX 76129, USA

T.J. McCoy
Department of Mineral Sciences, Smithsonian Institution, Washington, DC 20546, USA

their properties are critical for instrument calibration and interpretation of Vesta's geologic history.

Keywords Meteorites · Vesta · Asteroid · Eucrite · Diogenite · Howardite

1 HED Connections to Vesta

1.1 Spectra and Orbital Dynamics

4 Vesta has been described as the smallest terrestrial planet (Keil 2002)—the only known intact asteroid inferred to have a metallic core, an ultramafic mantle, and a basaltic crust. The Dawn mission will greatly expand our understanding of this differentiated body, but arguably it is already the most intensely studied planetesimal. Vesta is thought to be the parent body of ~ 900 named HED (howardite-eucrite-diogenite) meteorites, by far the most voluminous group of achondrites (igneous meteorites). Laboratory analyses of their mineralogy and petrology, major and trace element chemistry, and stable, radiogenic, and cosmogenic isotopes provide geologic insights and constraints on their parent body that are unrivaled for any extraterrestrial object except the Moon.

Before reviewing what the HEDs reveal about Vesta's geologic history, we briefly summarize the evidence that links them to this asteroid. The original connection was drawn from the similarity in spectral reflectance between Vesta and eucrites (McCord et al. 1970). Subsequently, more detailed spectroscopic studies have supported this connection, and spectra taken as Vesta rotates show different regions on the surface that appear to be dominated by eucrites, diogenites, and howardites (Binzel et al. 1997; Gaffey 1997). Vesta spectroscopy is considered elsewhere (e.g. Pieters et al. 2005).

Dynamical difficulties in transferring samples of impact debris from Vesta into Jovian and secular resonances (and thence into Earth-crossing orbits) have been overcome by the discovery of numerous < 10 km Vesta family asteroids ("Vestoids," which are dynamically linked to Vesta) having spectra similar to HEDs (Binzel and Xu 1993; Vilas et al. 2000; Burbine et al. 2001). The orbits of Vestoids extend between that of Vesta and both the 3:1 Jovian and $\upsilon 6$ resonances, which can act as escape hatches for samples from the main belt and allow trajectories into the inner solar system. Several V-type asteroids (spectrally similar to Vesta) of ~ 1.0–3.4 km diameter are in Earth-approaching orbits (Cruickshank et al. 1991). The dimensions of a huge impact crater at Vesta's south pole (Thomas et al. 1997) are consistent with the excavation of ~ 10^6 km^3 of rock, much more than needed to account for the Vestoids and other V-type near-Earth asteroids. Many HEDs probably derive from this crater, although other craters on Vesta likely supplied some meteorites.

1.2 Are All HEDs from Vesta?

For many years Vesta appeared to be unique—the only sizeable main belt asteroid with spectra that matched HEDs. Recent discoveries of other bodies, such as Magnya and the Merxia and Agnia families with similar spectra (Lazzaro et al. 2000; Sunshine et al. 2004) allow the possibility that within the HED collection are samples from other differentiated asteroids. Because of the likelihood of Vesta sampling through migration of Vestoids into nearby resonances (Sect. 1.1), the bulk of HEDs are probably from Vesta, but there are reasons to suspect that a few meteorites are not.

Bodies, like Vesta, that have undergone large-scale or complete melting and differentiation are commonly thought to have had their oxygen isotopes homogenized so that their

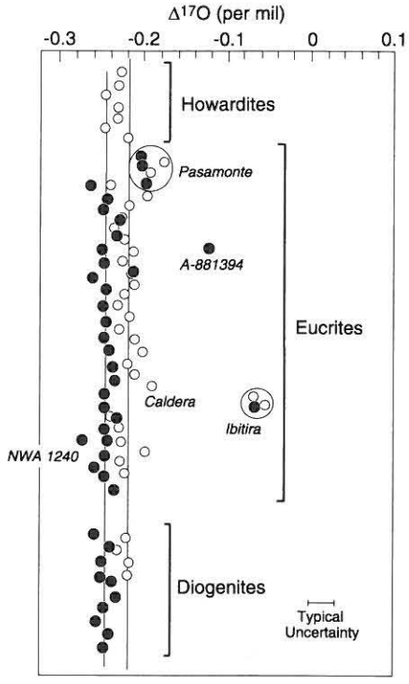

Fig. 1 Oxygen isotopic compositions, expressed as Δ^{17}O, for HED meteorites. *Open circles* and the *right-hand vertical line* (average value) are from Wiechert et al. (2004), and *solid circles* and the *left-hand vertical line* are from Greenwood et al. (2005). The names of isotopically anomalous meteorites are shown

various samples lie on a common mass-fractionation line. Indeed, the oxygen isotopic compositions of most HEDs, expressed as Δ^{17}O (the deviation of δ^{17}O and δ^{18}O from the terrestrial mass-fractionation line, which is assigned a value of 0) and illustrated in Fig. 1, are very similar. As a result, oxygen isotopes are commonly used to confirm the classification of HEDs. Figure 1 contains data from two laboratories; open symbols are from Wiechert et al. (2004) and filled symbols are from Greenwood et al. (2005) and Scott et al. (2009a). The two data sets give slightly different average Δ^{17}O values, indicated by the vertical lines, possibly due to different methods of correcting data to the internationally accepted standard. In any case, Fig. 1 illustrates remarkably little deviation from the mean value, although a few eucrites are clearly aberrant (the most obvious are identified by their italicized names). All the diogenites have Δ^{17}O values consistent with most eucrites, and small deviations in some howardites can be explained by foreign (chondritic) inclusions. Different interpretations of the eucrite deviations have been proposed. Wiechert et al. (2004) suggested that the anomalous samples indicated that the HED parent body was isotopically heterogeneous and thus had not melted completely. Greenwood et al. (2005) argued that the isotopic uniformity of most HEDs was evidence that the parent body had melted completely to form a magma ocean, and suggested that the one aberrant eucrite they analyzed was the result of projectile contamination. More recently, Scott et al. (2009a) proposed that all the eucrites with distinctive oxygen isotopic compositions are not from Vesta at all. Ibitira provides an interesting example. Not only is its oxygen isotopic composition distinctive (Fig. 1), but its vesicular texture is unusual, its abundances of alkali elements are lower, and its Ti/Hf ratio is higher than for other eucrites (Mittlefehldt 2005).

The Fe/Mn elemental ratios in pyroxenes and olivines have also been used to identify rocks with the same planetary parentage (Papike et al. 2003), because divalent iron and man-

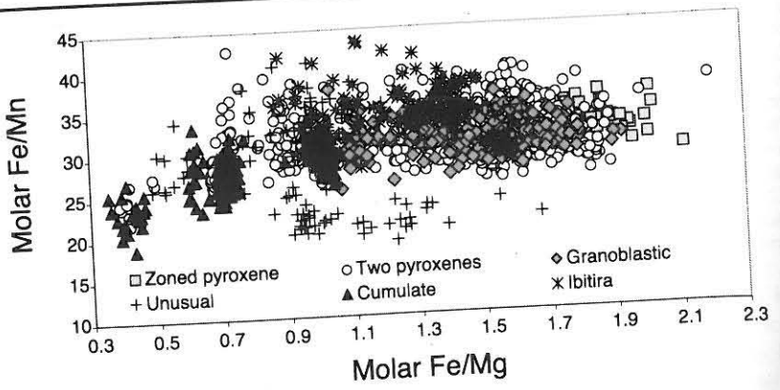

Fig. 2 Molar Fe/Mn and Fe/Mg ratios in unbrecciated eucrites, after Mayne et al. (2009). Fe/Mn has sometimes been used to indicate eucrites from a parent body distinct from Vesta

ganese are not expected to fractionate during planetary geologic processes. As with oxygen isotopes, most HEDs have similar Fe/Mn ratios in pyroxene and olivine (Papike et al. 2003; Beck and McSween 2008). Although Ibitira pyroxenes have higher Fe/Mn ratios than other eucrites, new data indicate that they overlap the Fe/Mn ratios of other eucrites (Fig. 2; Mayne et al. 2009). More precise data are needed to resolve differences in data sets. The issue is complicated, because most eucrites with distinctive oxygen isotopic compositions have normal Fe/Mn ratios, whereas at least one eucrite with distinctive pyroxene Fe/Mn has normal $\Delta^{17}O$.

Another potential problem is the suggestion that several other differentiated meteorite groups, specifically mesosiderites, main-group pallasites, and IIIAB irons, may have also originated on the HED parent body. Silicates in the main-group pallasites are distinct in $\Delta^{17}O$ from HEDs but mesosiderites are identical to them (Greenwood et al. 2006). No high-precision oxygen isotopic analyses have yet been reported for oxides in IIIAB irons to test their possible relationship. However, the petrologic properties of IIIAB irons and pallasites require their formation deep inside asteroids, and the very existence of core and core-mantle boundary meteorites appears to be at odds with the observation that Vesta is still intact. Most basaltic and orthopyroxenite clasts in mesosiderites are petrologically and chemically indistinguishable from eucrites and diogenites (Mittlefehldt 2005). However, mesosiderite silicates have undergone complex processing after metal-silicate mixing on the surface of their parent asteroid, and such processing is not evident in HEDs. Moreover, radiometric age data for a mesosiderite indicate that its parent body differentiated well after the HED parent body (Wadhwa et al. 2003). Finally, although only a portion of Vesta's surface has been observed spectroscopically, no areas have yet been found showing a spectrum like that of mesosiderites.

To minimize uncertainties, we will omit discussion of other meteorite types, and focus on the many HEDs that share the same oxygen isotopic compositions. We cannot, however, rule out the possibility that all HEDs are from the same, isotopically heterogeneous parent body.

2 Mineralogy, Petrology, and Magnetic Properties

All HEDs are igneous rocks or breccias composed of fragmented igneous rocks. The minerals that crystallized from magmas provide insights into the compositions of the melts and the processes that attended their solidification to form Vesta's crust. Classification of HEDs, along with descriptions of their textures and mineralogy, are essential elements for understanding their formation. Mineral compositions and proportions can also be compared with spectroscopic data to be obtained by Dawn.

2.1 Eucrites

The eucrites are believed to have crystallized as lavas on the asteroid's surface or within relatively shallow-level dikes and plutons. There are currently several different ways to subdivide the eucrites. The simplest of these classifications is based on petrology, which recognizes eucrites as either basaltic or cumulate rocks (Stolper 1977). Basaltic eucrites can be further subdivided by their geochemistry, as discussed in Sect. 3.

Eucrites are dominated by pyroxenes and plagioclase, with lesser amounts of metal, troilite, chromite, ilmenite, and silica. Other phases such as baddeleyite, zircon, fayalitic olivine, and phosphates are rare and tend to be found in the mesostasis. Most eucrites are brecciated.

Many basaltic eucrites are fine- to medium-grained, ophitic to subophitic rocks (Fig. 3a). However, this description does not encompass the wide range of textures seen within these basalts. At one extreme, the ALH 81001 eucrite exhibits a quenched vitrophyric texture with skeletal pyroxenes and a silica-plagioclase composition glass in place of crystalline plagioclase (Delaney et al. 1984; Mittlefehldt et al. 1998; Mayne et al. 2009). At the other extreme lie eucrites that have lost some of their igneous textures due to metamorphic recrystallization (Fig. 3b). This metamorphic overprinting occurs to differing degrees, from basaltic eucrites such as BTN 00300 and GRA 98098 still showing remnants of their ophitic igneous texture, to EET 90020 and LEW 85305 which have granoblastic pyroxenes. Vesicles are rare, but do occur (e.g. PCA 91007, Yamato 981651). These likely formed at depth due to the high efficiency of gas escape processes on an airless body such as an asteroid (McCoy et al. 2006).

The basaltic eucrites contain Fe-rich pyroxenes. Orthopyroxene, pigeonite, and augite are present, with the latter two predominating (Fig. 4). Basaltic eucrite pyroxenes crystallized as zoned pigeonites (Takeda and Graham 1991). However, in most cases thermal metamorphism has obliterated the original Mg-Fe zonation (Yamaguchi et al. 1996). As a result, the basaltic eucrites commonly contain low-Ca pigeonite hosts with finely exsolved augite lamellae (Mittlefehldt et al. 1998), so that electron microprobe beams overlap both phases and give intermediate compositions (Fig. 4). Igneous Ca zonation is sometimes preserved as a higher density of augite lamellae in grain rims compared to cores (Takeda and Graham 1991).

Plagioclase is calcic (An_{96-75}), and individual meteorites can show a wide range of compositions. For example, the plagioclases within Nuevo Laredo and Chervony Kut span almost the entire range seen within the basaltic eucrites, with compositions of An_{95-74} (Warren and Jerde 1987) and An_{94-75} (Mayne et al. 2009), respectively. Eucrites do not contain K-feldspar, with one notable exception: NWA 4523, a polymict basaltic eucrite found to contain small K-feldspar grains in mesostasis (Barrat et al. 2007). Warren and Gessler (2001) suggested that K-feldspar may occur in eucrite Bluewing 001, but this could also be K-rich glass.

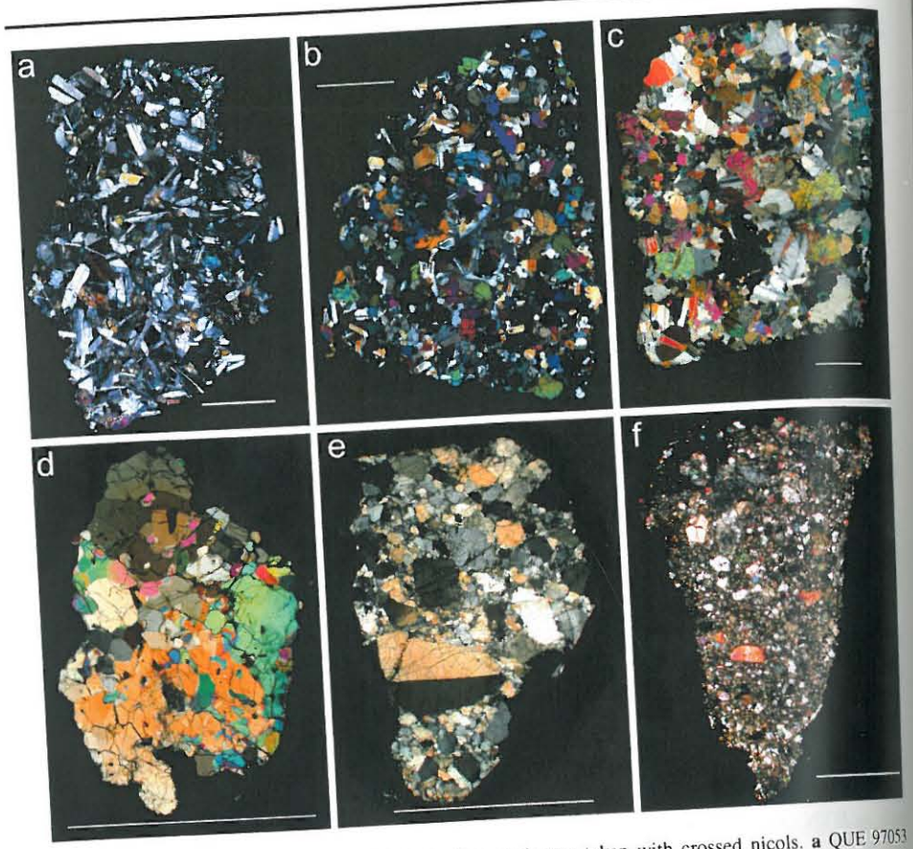

Fig. 3 Textures of HED meteorites; all photomicrographs are taken with crossed nicols. **a** QUE 97053 basaltic eucrite, with subophitic texture of plagioclase grains (*gray laths*) partly enclosed by pyroxene; **b** metamorphosed EET 90020 basaltic eucrite, with recrystallized texture; **c** Moore County cumulate eucrite; **d** GRA 98108 olivine diogenite; **e** QUE 99050 diogenite, with brecciated texture; **f** PCA 02019 howardite, a breccia composed of eucrite and diogenite clasts. All scale bars are 2.5 mm

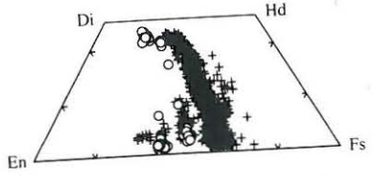

Fig. 4 Compositions of pyroxenes in eucrites. Crosses are exsolved pyroxenes (pigeonite and augite) in unbrecciated basaltic eucrites, and open circles are pyroxenes in cumulate eucrites. Basaltic eucrites appear to have pyroxene compositions that span the range from orthopyroxene, through pigeonite, to augite. However, basaltic eucrites actually only contain orthopyroxene to low-Ca pigeonite hosts with finely exsolved augite lamellae and, as a result, the electron microprobe beam often overlaps both phases, giving an intermediate pigeonite composition. Adapted from Mayne et al. (2009)

Silica minerals occur in proportions ranging from 0 to >10% (Mayne et al. 2009). Cristobalite, tridymite, and quartz have all been identified (Delaney et al. 1984; Yamaguchi et al. 2001; Chennaoui Aoudjehanne and Jambon 2007). Tabular shaped silica grains that over-

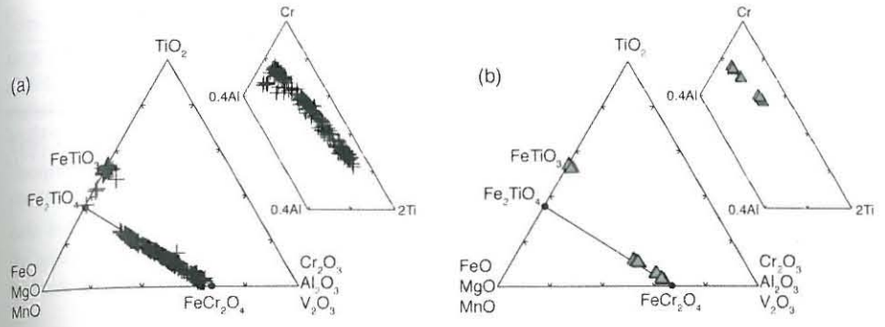

Fig. 5 Compositions of spinels and ilmenite in eucrites. Oxides in **a** basaltic eucrites, and **b** cumulate eucrites. Adapted from Mayne et al. (2009)

grow or enclose the surrounding grains occur mostly in granoblastic eucrites. They tend to be < 2 mm in size, but in GRA 98098 they are > 1 cm (Mayne et al. 2009). Yamaguchi et al. (1997) suggested that the prevalence of these grains in granoblastic eucrites may result from partial melting. Barrat et al. (2007) observed that mesostasis is absent from basaltic eucrites that are believed to have undergone high-temperature processing up to the point where partial melting occurred, and postulated that the partial melts were removed from these rocks. Therefore, the tabular silica grains may reflect melt recrystallization. However, some relatively unmetamorphosed basaltic eucrites contain tabular silica within mesostasis, suggesting a different mode of formation (Buchanan et al. 2000; Mayne et al. 2009).

Chromites show a range of compositions, which span most but not all of the ulvöspinel-chromite solid solution series (Fig. 5; Mayne et al. 2009). Ilmenite also is compositionally variable, with ilmenite MgO contents ranging from 0.3 to 5.2 wt% and Cr_2O_3 from 0 to 5.5 wt% (Mayne et al. 2009).

Cumulate eucrites, unlike their basaltic counterparts, are predominantly unbrecciated (Mittlefehldt et al. 1998), although cumulate eucrite clasts have been identified within polymict eucrites (Takeda 1991; Lindstrom and Mittlefehldt 1992). Texturally, the cumulate eucrites are not as diverse as the basalts. They are equigranular gabbroic rocks (Mittlefehldt et al. 1998). They are generally coarser-grained than their basaltic counterparts, although there is some variation in grain size (Fig. 3c).

The cumulate and basaltic eucrites are very similar mineralogically, in that they consist primarily of pyroxene and plagioclase. Pyroxenes in cumulate eucrites are more Mg-rich (Fig. 4). Although both low-Ca pyroxene and augite are present as a result of exsolution from pigeonite, modally there tends to be less augite than in the basaltic eucrites. Cumulate eucrites also show a much narrower range of plagioclase compositions, An_{90-96} (Mittlefehldt et al. 1998; Mayne et al. 2009). The metal is kamacite, low in both Co and Ni (< 1%). The scales of compositional variations in chromite and ilmenite in the cumulate eucrites are considerably less than in the basaltic eucrites (Fig. 5; Mayne et al. 2009). Some silica minerals are also present but usually in small amounts. Serra de Magé is the only eucrite in which quartz has been identified (Treiman et al. 2004).

Most eucrites, whether basaltic or cumulate, show evidence of thermal metamorphism. The effect of metamorphism on major element pyroxene chemistry was documented by Takeda and Graham (1991), who divided the eucrites into six types reflecting increasing degrees of equilibration. Yamaguchi et al. (1996) later added an additional type 7. Unmetamorphosed (type 1) eucrites preserve all their original pyroxene zonation and increasing

metamorphism results in homogenization through Fe-Mg diffusion, giving rise to a homogeneous pigeonite host exsolving augite lamellae (Takeda and Graham 1991). Eucrites with homogenized pyroxenes (types 4–7) are known as 'equilibrated' (Takeda and Graham 1991; Yamaguchi et al. 1996), but this designation refers only to pyroxene major elements. The kinetics of Fe-Mg diffusion in pyroxene are faster than those of Si-Al in plagioclase (O'Neill and Delaney 1982), and equilibrated eucrites can have a wide range of plagioclase compositions (e.g. Hsu and Crozaz 1996). In a study of the unbrecciated eucrites, Mayne et al. (2009) observed that along with variations in plagioclase content, many equilibrated eucrites also showed remnants of original minor element (Al, Ti, Cr) zonation in pyroxenes. Using all three of these components provides a more sensitive guide to the relative degree of thermal metamorphism a eucrite has experienced.

2.2 Diogenites

The diogenites are coarse-grained cumulates that are traditionally believed to have originated from a plutonic layer deep in the crust. However, complex thermal histories and brecciation have obscured some primary features used to interpret their origin. Recent studies showing both petrologic and geochemical variations among the diogenites suggest that their petrogenesis may have been more complex than previously thought.

Most diogenites are nearly monomineralic, being composed almost entirely of orthopyroxene (87–99%). Chromite and olivine generally occur in minor amounts (<10%). Accessory phases in diogenites include troilite (0–3%), plagioclase (0–3%), diopside (0–2%), silica (0–2%), metal (≤ 1%), and rare phosphates (Bowman et al. 1997). Due to the brecciation of diogenites, significant amounts of plagioclase and diopside can be attributed to the incorporation of eucrite fragments. For example, sections of ALH 85015 and PCA 02008 contain small basaltic (plagioclase + diopside) clasts comprising 9.8% and 8.6% of the samples, respectively (Beck and McSween 2010). The pairing of PCA 02008 with several PCA 02 howardites, coupled with the presence of eucritic fragments, suggests that PCA 02008 likely represents a diogenite-rich fragment of what was a larger, howardite-like meteoroid (Welten et al. 2009). The same may be true for ALH 85015, which contains components appearing howardite-like (Berkley and Boynton 1992) and others that are diogenitic (Score and Mason 1986, Beck and McSween 2010).

One significant variation from this mineralogy is that a number of diogenites contain significant amounts of olivine. Sack et al. (1991) discovered large amounts of olivine in ALHA 77256 (35%) and EETA 79002 (27%). These two olivine-rich samples, dubbed "olivine diogenites" (Fig. 3d), were hypothesized to represent mantle residues from partial melting. However, other sections of these diogenites do not contain abundant olivine (Bowman et al. 1997; Mittlefehldt 1994), and the orthopyroxene compositions of ALHA 77256 and EETA 79002 are not distinct from those in other diogenites (Fowler et al. 1994, 1995). These findings suggest that olivine diogenites are not residues, but cumulate rocks akin to other diogenites. Further insight comes from the discovery of harzburgite (olivine + magnesian orthopyroxene rock) clasts in brecciated olivine-bearing diogenites (Beck and McSween 2010). These clasts, which resemble olivine diogenites both texturally and chemically, are distinct from conventional (ferroan orthopyroxene) diogenites. Harzburgite and orthopyroxenite may have formed through fractional crystallization in multiple plutons (Beck and McSween 2010). The dunite breccia MIL 03443 resembles HEDs in texture, siderophile element abundances, and mineral chemistries. This sample may represent a partial melt residuum from the mantle of Vesta or a crustal cumulate (Krawczynski et al. 2008; Mittlefehldt 2008).

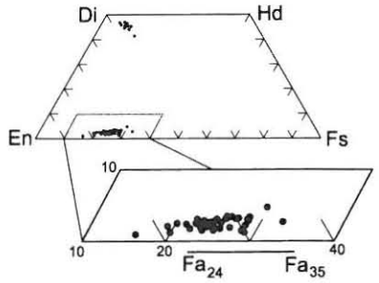

Fig. 6 Compositions of pyroxenes and olivines in diogenites. Data from Domanik et al. (2004), Fowler et al. (1994), Mittlefehldt (1994, 2000), and Mittlefehldt and Lindstrom (1993)

LEW 88679 and Tatahouine appear unbrecciated and display polygonal textures. However, most diogenites are brecciated to some degree. This can present a challenge in interpreting primary textures and deducing primary petrologic information. Diogenite textures are broadly described as having large, subhedral orthopyroxene clasts set in a finer, fragmental matrix dominated by orthopyroxene (Fig. 3e). Based on the largest reported intact orthopyroxene grain, ~ 5 cm (Mason 1963), the initial grain size for some diogenites must have been at least this large. Most minor and accessory phases occur as poikilitic inclusions within larger orthopyroxene clasts. Opaque grains (troilite, metal, and chromite) are often found as 1–10 μm circular blebs, aligned into "curtains." These lineaments are thought to represent relict grain boundaries or healed fractures in orthopyroxene grains (Gooley and Moore 1976). Diopside occurs as ~ 1 μm-thick exolution lamellae in orthopyroxene. Minor phases can also occur as separate, subhedral grains in the fragmental matrix. Olivine and chromite are exceptional among the minor minerals in that they can occur as mm-sized, subhedral grains (Irving et al. 2003; Mittlefehldt et al. 1998; Righter 2001; Sack et al. 1991).

Diogenite pyroxenes have a narrow range in major element concentrations (Domanik et al. 2004; Fowler et al. 1994; Mittlefehldt et al. 1998; Mittlefehldt 2000; Mittlefehldt and Lindstrom 1993). Except for a few compositionally unusual diogenites, pyroxene compositions fall within Wo_{1-3} En_{71-77} Fs_{22-24} (Fig. 6). The homogeneity in major element (Mg and Fe) compositions is believed to be the result of post-crystallization equilibration, not igneous fractionation (Fowler et al. 1994; Mittlefehldt 1994). Several clusters of pyroxene mg#s (defined as molar $100 \cdot Mg/(Mg + Fe)$) among the suite (Harriott and Hewins 1984; Mittlefehldt 1994) may represent separate equilibrated source regions, or different parts of a single diogenite reservoir that did not fully equilibrate (Fowler et al. 1994; Mittlefehldt 1994). Because this equilibration occurred prior to brecciation and mixing, it is possible for a single sample to contain pyroxenes with a range in mg#s (Mittlefehldt 2000).

Pyroxene minor and trace elements have not been affected in the same manner as the major elements. Their relatively low diffusivities allowed for the preservation of initial compositional trends during equilibration, and thus can be used to infer primary igneous processes. In most diogenites, minor incompatible elements (Sc, Al, Ti and Yb) vary considerably. These ranges necessitate a formation process in which (1) a single undepleted source underwent 60-90% fractional crystallization, (2) a depleted magma chamber, where plagioclase has been removed, underwent significantly less fractional crystallization, or (3) multiple magma chambers with varying incompatible element abundances underwent fractional crystallization separately (Fowler et al. 1995; Mittlefehldt 1994). The third option, multiple magma chambers, has gained further momentum from bulk diogenite REE analyses (Barrat et al. 2008; Mittlefehldt et al. 2009). The abundance of chromium, a minor compatible element, also varies in diogenite pyroxene. Like the incompatible elements, chromium and

other compatible minor elements are usually decoupled from orthopyroxene mg# (Berkley and Boynton 1992; Fowler et al. 1994).

Fe-Mg ordering has been measured in diogenite orthopyroxene, in an attempt to discern cooling rates and infer depths of burial. Using X-ray diffraction, Zema et al. (1997) determined closure temperatures ranging from 311 ± 29°C to 408 ± 10°C in seven diogenites. Cooling rates calculated from these temperatures are ~ 50°C/kyr to 800°C/kyr, respectively (Zema et al. 1997). The majority of these temperatures fall below the closure temperature for the cumulate eucrite Serra de Magé, which was determined using the same method (Domeneghetti et al. 1995). This relative closure temperature difference supports a deep (lower crust?) origin of diogenite plutons. Sample-wide closure temperature variations may reflect different depths at which the diogenites were emplaced (Zema et al. 1997). Recent findings by Verma et al. (2008) imply that the cooling rates for diogenites may be even slower than previously reported. Their findings show that all the Fe^{2+} in diogenite pyroxene resides in the more ordered M2 crystallographic site, in contrast to Zema et al. (1997) who reported Fe^{2+} in the M1 site as well.

Olivine compositions in diogenites (Fig. 6) are confined to a small range: Fo_{70-73} (Floran et al. 1981; Mittlefehldt 1994; Sack et al. 1991). A few outliers exist; for example, LEW 88008 contains Fo_{65} olivine and EETA 79002 has Fo_{77-75} olivine (Beck and McSween 2010; Mittlefehldt 2000; Sack et al. 1991). Minor and trace elements in diogenite olivine are restricted to a narrow compositional range. Chromites, on the other hand, display significant chemical variations (Bowman et al. 1999; Floran et al. 1981; Mittlefehldt 1994; Sack et al. 1991), from Cr-rich/Al-poor spinel in LAP 91900 (60.7 wt% Cr_2O_3; 6.1 wt% Al_2O_3) to Cr-poor/Al-rich spinel in ALHA 77256 (44.7 wt% Cr_2O_3; 21.8 wt% Al_2O_3). Some variation exists in chromite Mg/(Mg + Fe), but as in pyroxene, these trends are decoupled from Al_2O_3 and Cr_2O_3 concentrations (Bowman et al. 1999). Plagioclase has calcic compositions (An_{86-82}) in diogenites (Mittlefehldt et al. 1998). FeNi metal compositions range from 1.5 to >50 wt% nickel, and cobalt varies from 0.11 to 27.3 wt% (Gooley and Moore 1976). This large range in metal compositions, like the variations observed in pyroxene minor elements, might be attributed to different source regions for the diogenites (Gooley and Moore 1976) or possibly to contamination.

2.3 Polymict Breccias

Following the formation of Vesta's igneous crust, impacts excavated igneous rocks from various crustal levels. Impact mixing of eucritic and diogenitic lithologies has produced a range of polymict breccias, including the polymict eucrites and the howardites (Mittlefehldt et al. 1998). Unlike their monomict counterparts, these meteorites are distinguished by containing clasts of clearly distinct petrogenetic origin. Howardites are typically described as mixtures of eucritic and diogenitic clasts (Fig. 3f). Polymict eucrites were originally defined as containing different types of eucritic clasts (e.g. basaltic and cumulate; Miyamoto et al. 1978). The definition was later changed to encompass breccias with up to 10% diogenitic material; above that level the meteorite would be classified as a howardite (Delaney et al. 1983). Application of such a classification is problematic in the study of coarse-grained igneous rocks using thin sections (areas typically ~ 1 cm^2). In fact, the distinction between howardites and polymict eucrites is arbitrary and these definitions have been applied inconsistently. Current sampling suggests that there is essentially a continuum from unbrecciated eucrites, through monomict and polymict eucrite breccias, to howardites and polymict diogenite breccias, and finally to unbrecciated diogenites. This gradation is not surprising, given the impact fragmentation and mixing that occurred on an asteroidal scale.

The igneous clasts in polymict eucrites and howardites are similar to their unbrecciated counterparts already described. There are, however, important exceptions that testify to a broader array of lithologies than are sampled as individual meteorites (Delaney et al. 1984; Bunch and Rajan 1988; Mittlefehldt et al. 1998). Some of these distinctive clasts (e.g., plagioclase-rich, quartz-normative, hypersthene-rich) are distinguished on the basis of modal mineralogy and may simply be small, unrepresentative areas from coarse-grained eucritic lithologies. Other clasts show clear differences in mineral abundance and composition from known eucrites and diogenites, extending the range of fractionation seen among HEDs. Ikeda and Takeda (1985) described a small, unusually ferroan clast in Y-7308 composed of fayalitic olivine (Fa_{86-90}), hedenbergitic pyroxene ($Fs_{40-43}Wo_{41}$), tridymite, and plagioclase (An_{78-85}) with minor ilmenite, chromite, troilite, iron metal, and whitlockite. This clast was ascribed to late-stage crystallization from a fractionating magma. In contrast, Mittlefehldt and Lindstrom (1997) studied dark glassy clasts from howardites EET 92014 and Kapoeta that contain more Mg-rich pyroxenes than are typically seen in the cores of zoned basaltic eucrite pyroxenes. They suggested that these magnesian basalt clasts originated as impact melts of howardite, rather than as primary melts of a more magnesian source region than that which produced basaltic eucrites. Treiman and Drake (1985) described ferroan troctolite (olivine + plagioclase) in ALHA 80102.

The suggestion that impacts may have produced some of the 'igneous' clasts in howardites is consistent with other lines of evidence. A subset of the howardites is enriched in solar-type noble gases that are concentrated on the surfaces of mineral and glass fragments (Rao et al. 1991). These gases were implanted when the grains resided in the upper ~ 1 m of the regolith. The gas-rich howardites are also enriched in fragments of meteoritic impactors and of impact melts. Chondritic clasts are a common, if volumetrically minor, component of howardites. Most chondritic clasts are similar to the hydrated, phylosilicate-bearing CM2 chondrites, although clasts similar to CR2, metamorphosed CI, and CV3 chondrites are also known (Zolensky et al. 1996; Gounelle et al. 2003). Warren et al. (2009) noted that gas-rich howardites are also significantly enriched in siderophile elements (e.g. nickel and iridium) compared to gas-poor howardites. Buchanan et al. (2009) reached a similar conclusion, noting high siderophile abundances in most HED polymict breccias, even in the absence of observable foreign clasts. The siderophile enrichment is attributed to incorporation of meteoritic materials ranging from recognizable clasts to submicroscopic mineral grains. Impact melt particles range from spherical to irregular in shape and include both glass and devitrified glass (Bunch 1975; Olsen et al. 1990). Olsen et al. (1990) noted that the bulk composition of glasses found in howardites is generally similar to the bulk meteorite composition, but that silica-rich glasses are present in Monticello and Y-7308. Barrat et al. (2009) discovered glass spheres in howardites enriched (up to 6 wt.%) in K_2O. Both papers suggest that these unusual glasses represent shock-melts of previously unsampled rock types from the HED parent body. It is unclear whether such lithologies are small, late-stage segregations from a crystallizing magma, akin to the ferroan clast in Y-7308, or might sample larger terranes, perhaps analogous to the lunar KREEP terrane. Siderophile element enrichments, foreign fragments, and impact melt spherules can serve as proxies for regolith exposure, even in the absence of measurements of noble gas enrichments. Warren et al. (2009) proposed that howardites exhibiting these characteristics be classified as a distinct subclass—regolithic howardites. Conversely, howardites and polymict eucrites that lack these signatures, although formed by brecciation and mixing of primary igneous lithologies, may not have been exposed within the upper meter of the regolith.

As a group, polymict breccias from the HED group provide a broad sampling of, and invaluable insights into, their parent body. If we accept that most HED meteorites originated

on Vesta, the characteristics of igneous clasts in polymict breccias are essential to understanding the petrologic diversity of that asteroid and, by extension, the geologic processes that shaped it. Spectral observations (e.g. Binzel et al. 1997; Gaffey 1997) suggest that much of the surface of Vesta resembles the howardites in mineralogy and bulk chemical composition.

2.4 Magnetic Anisotropy

Magnetic anisotropy is a proxy for the bulk fabric of rocks. Magnetic measurements of HED meteorites (Collinson and Morden 1994; Gattecceca et al. 2008) demonstrate that eucrites, diogenites, and howardites display similar mean anisotropy. However, the magnetic fabrics of eucrites are markedly oblate, those of diogenites are more neutral, and those of howardites are intermediate. Despite being breccias, the HEDs have strong and spatially coherent magnetic anisotropy, indicating that deformation occurred after the last brecciation. Gattecceca et al. (2008) attributed the magnetic fabrics in eucrites and diogenites to lithostatic compaction and thermal metamorphism, and the fabrics in howardites to hypervelocity impacts.

3 Geochemistry and HED Petrogenesis

As described above, the HED meteorite suite includes igneous rocks and polymict breccias composed of those lithologies plus exogenous materials accreted to the surface of the differentiated parent asteroid. Igneous rock compositions are determined by the compositions of the sources of their parent magmas and the processes that affected these magmas during melting and solidification. Incomplete melting is the rule in igneous systems, and the compositions of melts differ depending on the degree of partial melting. Crystals are commonly segregated from the liquid from which they grew (fractional crystallization), producing crystal aggregations (cumulates) and causing progressive changes in the composition of the remaining melt. Thus, study of the chemistry of igneous rocks from the HED parent asteroid provides information about the petrologic evolution of that body. The compositions of polymict breccias constrain the physical mixing process that occurred subsequent to formation of a solid crust.

Here we examine the geochemistry of HED meteorites with the goals of constraining the igneous processes responsible for differentiation of the asteroid and its later impact history. We begin by evaluating the compositions of eucrites (basalts and cumulate gabbros) in light of the vast body of new compositional data available for these rocks. After reinterpreting the basaltic suite, we consider in turn the diogenites and polymict breccias. We utilize the best averages calculated from data available in 286 literature sources and our unpublished data. We discuss a wide range of elements that provide strong constraints on igneous and mixing processes, even though the GRaND instrument on Dawn will analyze a much more restricted set of elements. Usui and McSween (2007) provide an example of how GRaND analyses might be used to identify HED compositions on Vesta.

3.1 Geochemistry of Eucrites and Basaltic Magma Series

The first modern attempt at interpreting the formation of HED meteorites was based on meteorite petrology (Mason 1962, 1969). He suggested that pallasites, diogenites, howardites and eucrites could be considered a differentiation sequence formed on a once-molten asteroid. Iron metal and olivine crystallized from the molten asteroid to form a core (pallasites).

Silicate crystallization switched to magnesian orthopyroxene, forming a mantle (diogenites), followed by crystallization of ferroan pyroxenes and plagioclase to form a mafic crustal layer (howardites), and ultimately the residual melt crystallized as gabbros (cumulate eucrites) or quenched in the near-surface environment (basaltic eucrites).

Crystallization models held sway until Stolper (1977) performed melting experiments on basaltic eucrites and showed that at low pressure and moderately reducing conditions, some eucrites were multiply saturated on their liquidi with pigeonite, ± olivine, spinel, plagioclase and metal. He interpreted these meteorites as representing primary partial melts. Other basaltic eucrites had compositions that resembled experimental melts after varying amounts of pyroxene and plagioclase crystallization. Stolper (1977) interpreted these as representing evolved melts formed after equilibrium or fractional crystallization of primary partial melts. Using major element data available at that time, he concluded that Stannern, Ibitira, Sioux County, and Juvinas formed a suite of primary partial melts, whereas the other eucrites he studied were residual melts from crystallization of either Sioux County- or Juvinas-like precursors. No eucrites were identified as residual melts from Stannern-like or Ibitira-like precursors.

Consolmagno and Drake (1977) modeled the rare earth element (REE) contents of basaltic eucrites. They found that the REE patterns of Stannern, Sioux County, and Juvinas could be modeled as primary partial melts of a primitive source as interpreted by Stolper (1977). However, they also modeled most other basaltic eucrites as primary partial melts, in contrast to Stolper's (1977) interpretation that they represent residual melts. Consolmagno and Drake (1977) found that the REE patterns of cumulate eucrites are consistent with formation as pigeonite-plagioclase cumulates from basaltic eucrite magmas, consistent with Stolper's (1977) interpretation.

Figure 7 summarizes compositional signatures of eucrites that support Stolper's interpretation. Figure 7a is a replica of the Ti versus mg# diagram used by Stolper (1977) to illustrate his petrogenetic scheme (he actually used fe# as the x-axis; plotting mg# in reverse order is equivalent). Titanium is an incompatible element in basaltic magmas. During partial melting, Ti is quantitatively partitioned into the first-formed melts, and continued melting dilutes Ti in the melt. During basaltic magma crystallization, the minerals formed are Ti-poor, resulting in increasing Ti in the residual melts as crystallization proceeds. The mg# of a partial melt is buffered by olivine in the source region and thus undergoes only a slight increase as melting proceeds. During crystallization the mg# steadily decreases as Mg-rich mafic minerals (olivine and/or pyroxene) crystallize from the melt. The partial melting trend, known in HEDs as the Stannern-trend, shows decreasing Ti with little change in mg# from the eponymous Stannern through Ibitira to the most primitive (highest mg#, lowest Ti) main-group eucrite Sioux County. The fractional crystallization trend, known in HEDs as the Nuevo Laredo-trend, shows increasing Ti with decreasing mg# going from main-group eucrite Sioux County to the eponymous Nuevo Laredo. (Because the Nuevo Laredo-trend emanates from the compositional space of main-group eucrites, we will refer to this trend as the main-group—Nuevo Laredo-trend.)

A trace incompatible element such as Hf substituted for Ti on Stolper's diagram (Fig. 7b) still shows the distinction between Stannern and most other eucrites, but note that Ibitira is no longer intermediate between Stannern and Sioux County. The distinction between Stannern and the main-group—Nuevo Laredo-trend eucrites is maintained if Sc (distribution coefficient of 0.5 to 1) is used instead of mg# (Figs. 7c, d). Note that on the Ti or Hf versus Sc diagrams the Stannern-trend (Stannern through Ibitira) does not intersect the main-group—Nuevo Laredo-trend at the most primitive (lowest Ti, Hf and Sc) ends.

Since Stolper presented his interpretation of eucrite petrogenesis, many new HED meteorites have been recovered, the number of chemical analyses available has dramatically

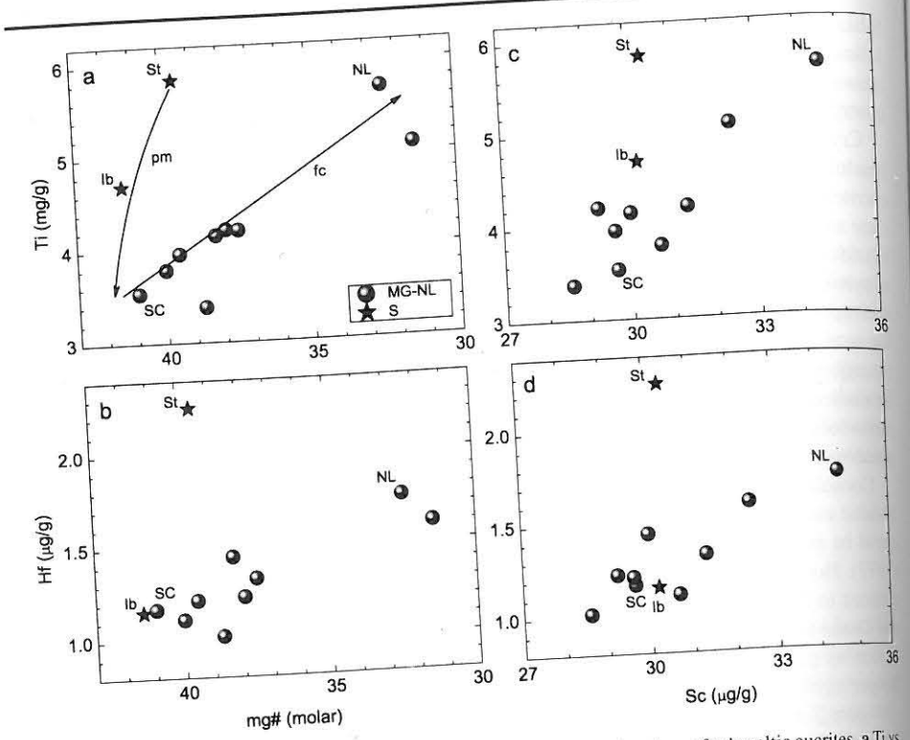

Fig. 7 Compositional representations of the Stolper (1977) petrogenetic scheme for basaltic eucrites. **a** Ti vs. mg# diagram showing the partial melting (pm) and fractional crystallization (fc) trends identified by Stolper (1977). Subsequent usage has termed these the Stannern-trend (S) and main-group—Nuevo Laredo-trend (MG-NL), respectively. Labeled meteorites are Ibitira (Ib), Nuevo Laredo (NL), Sioux County (SC) and Stannern (St). **b** The same trends are evident if the incompatible element Hf is substituted for the incompatible element Ti. Note however, that Ibitira is no longer intermediate in the partial melting trend. **c**, **d** The meso-compatible element (distribution coefficient = 0.5–1) Sc can be substituted for mg# to define the differences between partial melting and fractional crystallization. The meteorites shown in all panels are those considered by Stolper (1977). The Ti and mg# data are those used by Stolper (1977), whereas the Hf and Sc data are averages of all data available for the meteorites shown

increased and their quality has improved, changes in classification have been made for some HEDs, and more experimental work has been done. Thus, it is necessary to reexamine the chemical classification and interpretation of basaltic eucrites in light of these new data.

Figure 8 presents Ti versus mg# and Hf versus Sc diagrams for basaltic eucrites using averages of available eucrite data. As first shown by Barrat et al. (2007), two distinct data clusters appear on these diagrams. The low Ti, Hf cluster encompasses eucrites that formed the original main-group—Nuevo Laredo-trend and we retain that name for this cluster. The Ti- and Hf-rich cluster includes Stannern. Although a partial melting trend as originally posited by Stolper (1977) is no longer obvious, we apply the Stannern-trend name to this cluster, as did Barrat et al. (2007). Pomozdino has an anomalously high mg# (Fig. 8a). This rock is interpreted to be a partial cumulate, i.e. a cumulate containing an unusually high amount of trapped intercumulus melt (Warren et al. 1990). Its high mg# is a result of accumulation of pyroxene, while its incompatible trace element contents (Fig. 8b) reflect those of the trapped melt. Petrologic studies have not identified other partial cumulates among the

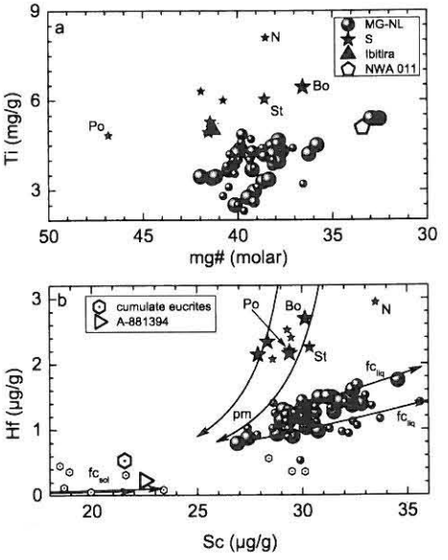

Fig. 8 Updated compositional representations of basaltic eucrite chemical types. **a** Ti vs. mg# diagram. Shown are averages of available data for all basaltic eucrites, plus the ungrouped basaltic achondrites Ibitira and Northwest Africa 011. Pomozdino (Po) has a high mg# because it is a partial cumulate (Warren et al. 1990). **b** Hf vs. Sc diagram. Cumulate eucrites and ungrouped cumulate gabbro A-881394 are also shown. A partial melting model (pm arrow) that previously matched Stannern-trend eucrites Bouvante (Bo) and Stannern (St), and the main-group eucrites does not adequately account for the most trace-element-poor Stannern-trend eucrites, and a model that passes through the latter does not match the compositions of main-group eucrites. With the additional data now available, the main-group—Nuevo Laredo-trend eucrites may represent two or more fractional crystallization sequences, and the Stannern-trend may represent a fractional crystallization sequence (fc_{liq} arrows). Some cumulate eucrites are broadly consistent with crystalline material fractionated from basaltic eucrites (fc_{sol} arrows). Also labeled is NWA 4523 (N) with anomalously high Ti and Sc (Barrat et al. 2007). Symbol sizes are correlated with the degree of confidence in the average: *large symbol*—standard deviation is $\leq 10\%$; *medium symbol*—standard deviation is $> 10\%$ and $\leq 20\%$; *small symbol*—standard deviation is $> 20\%$ or only a single analysis is available

basaltic eucrites, and the unique nature of Pomozdino is further supported by the lack of other examples with anomalous mg# (Fig. 8a).

As was the case in Fig. 7, Ibitira falls within the Stannern-trend on the Ti versus mg# diagram (Fig. 8a) but within the main-group—Nuevo Laredo-trend on the Hf versus Sc plot (Fig. 8b). We noted earlier that Ibitira is on outlier in $\Delta^{17}O$ (Wiechert et al. 2004) and that it also has several petrologic and compositional characteristics that are distinct from other basaltic eucrites (Mittlefehldt 2005). Ibitira is therefore considered an ungrouped basaltic achondrite and may not be from Vesta. A second ungrouped basaltic achondrite, NWA 011, shows petrologic and chemical similarities to basaltic eucrites, but is distinct from them in detail (Yamaguchi et al. 2002).

It is possible that the main-group—Nuevo Laredo-trend is actually a composite of two or more fractionation trends. The data distribution shows considerable variation in Ti at similar mg#, and variation in Hf at similar Sc content, that can be explained by distinct fractionation trends starting from different parent magmas (Fig. 8b). The Stannern-trend no longer shows a distribution compatible with partial melting. Barrat et al. (2007) have modeled Stannern-trend eucrites as being hybrid melts. In their model, magmas similar to main-group eucrites

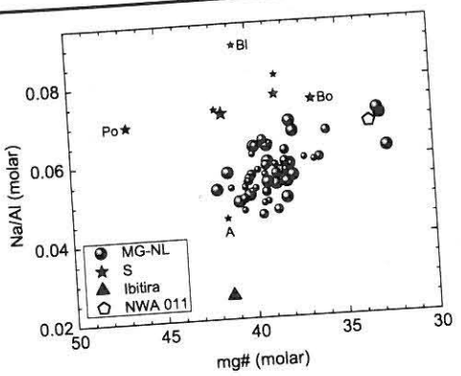

Fig. 9 Plot of molar Na/Al vs. mg# for bulk-rock basaltic eucrites, plus the ungrouped basaltic achondrites Ibitira and NWA 011. The main-group—Nuevo Laredo-trend eucrites correspond to trend A, and Stannern-trend eucrites correspond to trend B of Ikeda and Takeda (1985). Pomozdino (Po) has a high mg# because it is a partial cumulate (Warren et al. 1990). Ferroan Bouvante (Bo) plots close to the field of main-group—Nuevo Laredo-trend eucrites. ALHA 81001 (A) is anomalous compared to other Stannern-trend eucrites; it also has a unique, fine-grained quenched texture (see text). Bluewing 001 (Bl; analysis by Warren et al. 2009) has a higher Na/Al than any other basaltic eucrite. The significance of the relative sizes of the data points is as given in Fig. 8

interact with a hot crust of earlier generation main-group—Nuevo Laredo-trend eucrites. The magma causes partial melting of the hot crust, and mingling of the magma with the anatectic melts yields hybrid magmas with the compositional signatures of Stannern-trend eucrites.

Cumulate eucrites can be modeled as crystalline materials separated from the fractionating basaltic eucrites (Fig. 8b). Some cumulate eucrites have Hf contents that are too high for pure cumulates, but these can be modeled as mixtures of cumulus phases and trapped melt (e.g. Mittlefehldt and Lindstrom 2003; Treiman 1997).

Petrologic study of basaltic clasts in howardites identified two trends based on the Ca content of plagioclase and the Mg content of low-Ca pyroxene (Delaney et al. 1981; Ikeda and Takeda 1985). One trend, the peritectic basalts of Delaney et al. (1981), matched the mineralogic compositions of main-group—Nuevo Laredo-trend eucrites. The evolved basalt trend overlapped data from Stannern, the main-group—Nuevo Laredo-trend eucrite Chervony Kut and some clast data from the main-group—Nuevo Laredo-trend eucrite Pasamonte (Delaney et al. 1981). Ikeda and Takeda (1985) referred to these two trends as A and B; we use this terminology because it does not presuppose a mode of origin.

A plot of bulk-rock molar Na/Al versus mg# (Fig. 9) is roughly equivalent to the mineral composition diagram (mole% anorthite in plagioclase vs. mole% enstatite in pyroxene) used by Delaney et al. (1981) and Ikeda and Takeda (1985) to divide basaltic eucrites into different trends. Sodium and Al are almost entirely contained in plagioclase, and the Na/Al ratio is an inverse function of the plagioclase anorthite content. Most of the bulk-rock Mg and Fe are contained in pyroxene, and bulk-rock mg# will be a function low-Ca pyroxene enstatite content as long as the basalt does not also contain primary augite, which is true of many basaltic eucrites. The chemical groups main-group—Nuevo Laredo-trend and Stannern-trend closely correspond to trends A and B of Ikeda and Takeda (1985). Stannern-trend basalts have higher Na/Al for a given mg# (Fig. 9), mimicking the more sodic plagioclase compositions of trend B basalt clasts from howardites (Delaney et al. 1981; Ikeda and Takeda 1985). An exception to this is ALHA 81001, which has a much lower

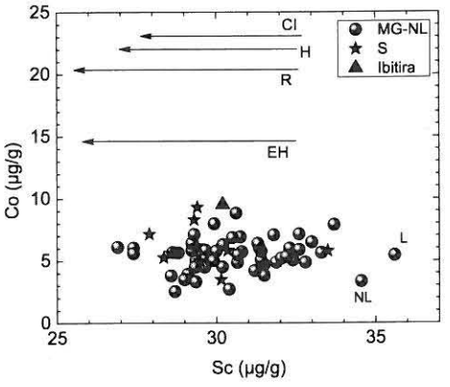

Fig. 10 Co vs. Sc for basaltic eucrites and Ibitira, compared with model partial melts (*arrows*). The partial melting models are based on chondrite Mg/Si and Fe/Si, but with Fe^0 and Fe^{2+} adjusted to yield a bulk silicate mg# of 64. Thus, the EH model, for example, has an EH Mg/Si and Fe/Si ratio, but is much more oxidized than a true EH chondrite. Chondrite compositions are taken from Lodders and Fegley (1998). Labeled eucrites: L—LEW 85305 (analysis by Mittlefehldt and Lindstrom 2003); NL—Nuevo Laredo

Na/Al than other Stannern-trend basalts. This rock also has a unique, quench texture that sets it apart petrographically from other basaltic eucrites (see Sect. 2.1). Bouvante plots close to the main-group—Nuevo Laredo-trend basalts, but nevertheless, has higher Na/Al than those main-group—Nuevo Laredo-trend basalts with similar mg#.

The partial melting model shown in Fig. 8b is one of a family of models that could explain trace element distributions for the Stannern-trend as it was known in 2003 (Mittlefehldt and Lindstrom 2003). Stannern and Bouvante fall along modeled partial melting tracks that intercept the main-group—Nuevo Laredo-trend eucrites at the primitive (low Sc, Hf) end of the sequence. However, with the addition of new meteorites, the partial melting model no longer satisfies the basaltic eucrite data. The model passes through the field of Stannern-trend eucrites, but many members have Sc and Hf contents that are too low (to the left of the partial melting model) to be plausible primary partial melts. Modeled tracks that pass through the low Sc, Hf Stannern-trend eucrites miss the low Sc, Hf end of the main-group—Nuevo Laredo-trend eucrites. Thus, it does not seem possible to construct a partial melting model based on simple assumptions (e.g. based on a chondrite-like source composition) to match trace lithophile element data for those basaltic eucrites that might be considered to be primitive melts based on their major element compositions.

Further evidence suggesting that partial melting models are incapable of matching basaltic eucrite compositions arises when siderophile element contents are evaluated. Early studies by Palme and Rammensee (1981), Newsom and Drake (1982), and Newsom (1985) showed that abundances of the refractory siderophile elements Mo and W in basaltic eucrites were inconsistent with equilibration with metal in a source region. These elements are partially lithophile. The same conclusion can be reached when considering other siderophile elements. For example, the Co contents of eucrites are a factor of ~ 3 times lower than a model that yields the lowest Co content for model melts (Fig. 10; see figure caption for a description of how the model sources are calculated). The Co contents of model melts are buffered by metal in the source region and thus do not vary during silicate partial melting; the melting temperature of Fe-rich metal is well above the silicate solidus. The model based on EH chondrites (Fig. 10) could yield Co contents like those of basaltic eucrites if the solid metal/silicate melt partition coefficient is ~ 3.5 times higher, or the parent body Co/Fe ratio

is ~ 2.5 times lower. Both options seem unlikely. The Co/Fe ratios of chondrites only vary by ~ 15% (Lodders and Fegley 1998), making the factor of 2.5 times lower Co in the parent asteroid implausible. Metal/silicate melt partition coefficients have been determined experimentally, and compensations for variations with temperature, pressure, melt composition, and oxygen fugacity can be calculated (Righter and Drake 1997). For the modeling shown, we used the partition coefficient of Holzheid and Palme (2007), which gives a closer approximation to the basaltic eucrite data than does the value used by Righter and Drake (1997) in their modeling. Parent asteroid compositions based on other model chondrite types (CI, H, R in Fig. 10) give even poorer fits.

3.2 Geochemistry of Diogenites and Complexities in Vesta's Differentiation

The discussion above on HED petrogenesis, and indeed most attempts at such modeling, are based on trying to explain the compositions and petrology of basaltic eucrites. A holistic approach to understanding Vesta's petrologic evolution requires incorporating diogenite petrology and composition into the modeling. Petrologic and compositional studies of diogenites have shown that in general, orthopyroxene grains are quite uniform in major element composition within individual diogenites (Fowler et al. 1994; Mittlefehldt 1994). Some diogenites do show variations in grain compositions. These variations are typically not continua, but distinct populations of grains from different source rocks in genomict or polymict breccias (Beck and McSween 2010; Fowler et al. 1994; Mittlefehldt 2000). In contrast to the uniformity in major elements, minor and trace incompatible element abundances are quite variable (Fowler et al. 1994, 1995; Mittlefehldt 1994). These studies have led to the conclusion that multiple parent magmas were responsible for diogenite formation (Fowler et al. 1995; Mittlefehldt 1994; Shearer et al. 1997). Some have raised the possibility that infiltration metasomatism may have caused the disconnect between major elements and trace elements, and the ranges in trace element contents in diogenite pyroxenes (Fowler et al. 1994). This process is too ill-defined to properly evaluate in the case of diogenites. Numerous diogenites have been recovered and analyzed since the mid 1990s, resulting in increased diversity in major element compositions and expanded ranges in minor and trace element compositions (Barrat et al. 2008). The trace element compositions in particular reveal that diogenite petrogenesis was complex.

Figure 11 shows averaged bulk rock compositions for Sm versus Sc for diogenites and MIL 03443. This latter meteorite is a brecciated dunite that appears to be related to diogenites (Krawczynski et al. 2008; Mittlefehldt 2008). Excluding the anomalous diogenite Dhofar 700 (Barrat et al. 2008), the diogenite suite exhibits a range in Sc contents from ~ 5.6 to ~ 22 μg/g and Sm varies by over a factor of 300. An example fractional crystallization model is also shown. This model is based on the "HED-EH" model of Ruzicka et al. (1997) which has an expanded range of low-Ca pyroxene crystallization and produces the maximum range in cumulate pyroxene trace element compositions of any of the models they considered. The partition coefficients used were calculated after Jones (1995).

The diogenite suite includes some members that have very low Sm (MET 00424, Tatahouine) or Sc (NWA 1461) contents that are out of the range achievable by model cumulates or their mixture with trapped melts. Most diogenites have Sc contents that can be modeled within the framework of the Ruzicka et al. (1997) HED petrogenetic scheme, but most contain more Sm than predicted by the fractional crystallization model (Fig. 11).

Two mechanisms can account for the high Sm contents of diogenites relative to the model cumulate: admixture of eucritic material in brecciated diogenites, or inclusion of trapped melt. Some diogenites are classified as being polymict breccias containing a small amount

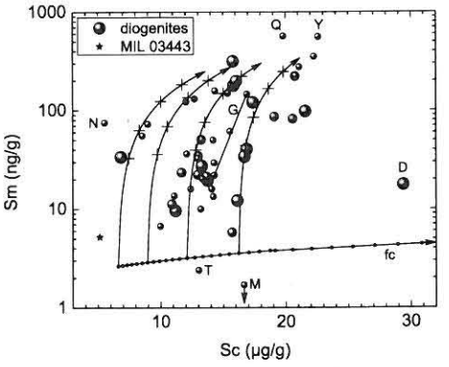

Fig. 11 Sm vs. Sc plot for diogenites and HED dunite MIL 03443 (analysis by Beck and Mittlefehldt, unpublished). A fractional crystallization model (fc) based on the "HED-EH" model of Ruzicka et al. (1997) is shown for comparison. *Curved arrows* show mixing between cumulate orthopyroxene and trapped melt, with the *tick marks* at 5, 10, 20 and 30% melt and the arrows terminating at 40%. Diogenites exhibit a wide range in incompatible trace element contents that are difficult to explain as cumulates plus trapped melt from a single parent melt. Labeled diogenites are Dhofar 700 (D; analysis by Barrat et al. 2008), Garland (G), MET 00424 (M), NWA 1461 (N; analysis by Warren et al. 2009), QUE 93009 (Q; Mittlefehldt, unpublished analysis), Tatahouine (T) and Y-791200 (Y; analysis by Warren et al. 2009)

of eucritic debris (Delaney et al. 1983). Mittlefehldt (1994) showed that for one of these, Garland, bulk-rock analyses were measurably contaminated with incompatible lithophile elements compared to an unbrecciated orthopyroxene-chromite clast (Fig. 11). However, another polymict diogenite, Aïoun el Atrouss, exhibits no significant difference between whole-rock and clast samples (Fig. 11). At present, petrographic study of diogenites to identify polymict breccias is incomplete, and therefore the potential for basaltic contamination in whole-rock analyses is incompletely known.

The incompatible trace element content of an orthopyroxenite cumulate will be dominated by a trapped melt component if present. Four mixing curves between orthopyroxenes and their equilibrium melts are shown to illustrate the effects of trapped melt on cumulate compositions (Fig. 11). The curves end at 40% trapped melt, and the tick marks are at 5, 10, 20 and 30%. Roughly half the diogenites can be explained as being cumulates with ≤ 5% trapped melt component. Some, however, would require >20% trapped melt. Large amounts of trapped melt should be revealed by higher modal plagioclase contents. There has not been a coordinated petrographic and compositional study of diogenites that might reveal systematic variations in trapped melt contents. Such a survey is needed to evaluate which may contain inordinately high trapped melt components.

In spite of these uncertainties, a model that forms all diogenites from a common parent magma (or magma ocean) seems inconsistent with variations in Dy/Yb, Sm/Yb, Sm/Sc, and Yb/Sc ratios (Barrat et al. 2008; Mittlefehldt et al. 2009). Diogenite petrogenesis appears to have been more complex than that inferred from basaltic eucrites.

3.3 Polymict Breccias and Impact Mixing

As described in Sect. 2.3, polymict breccias composed of fragmental material from multiple crustal units are important constituents of the HED collection. The compositions of polymict breccias provide clues to the mixing process and may reveal the presence of lithologies not sampled as individual meteorites.

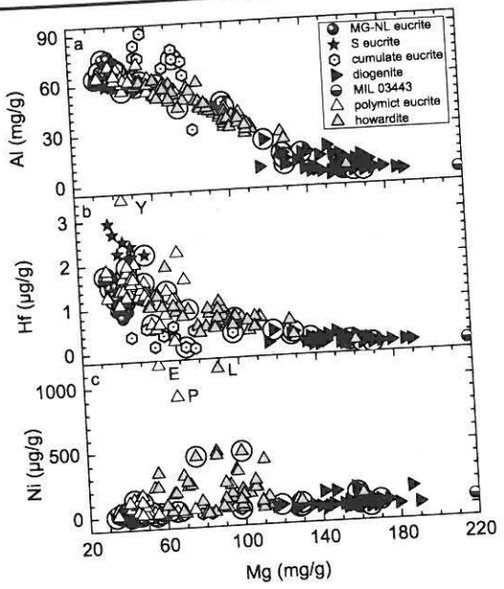

Fig. 12 Mixing diagrams for HED meteorites. **a** Polymict eucrites and howardites form an array between basaltic eucrites and diogenites in Al vs. Mg. Some, but not all, cumulate eucrites are distinct from this array. Circled meteorites are those whose cosmic-ray exposure ages lie within the age peak at ~ 22 Ma. **b** Hf vs. Mg diagram shows that some polymict breccias are dominated by Stannern-trend eucrites or cumulate eucrites. Labeled polymict eucrite is Y-75011 (Y). **c** Ni vs. Mg diagram shows that the polymict breccias are enriched in siderophile elements due to admixture of chondritic debris. Labeled meteorites are EET 92023 (E), LEW 85313 (L; analysis by Warren et al. 2009) and Petersburg (P). MIL 03443—unpublished analysis by Beck and Mittlefehldt

Figure 12a is a mixing diagram showing the relationship between Al and Mg in HED meteorites. Basaltic eucrites are rich in Al and poor in Mg, whereas diogenites have the opposite characteristics. All polymict breccias are consistent with simple mixtures of basaltic eucrites and diogenites (Fig. 12a). Stannern-trend basalts are not distinguished from main-group—Nuevo Laredo-trend basalts on this diagram. Some cumulate eucrites show high Al contents, but these are not reflected in polymict breccia compositions. Thus, based on major element compositions there is no clear evidence for howardites with significant cumulate gabbro components. Many cumulate eucrites do not show enhanced Al contents, however. Mixing diagrams using an incompatible trace element, such as Hf, show that some polymict eucrites and perhaps one howardite may be dominated by cumulate gabbros as their Al-rich component (Fig. 12b). Such cumulate gabbro-dominated polymict breccias are poor in Hf compared to howardites and polymict eucrites formed by mixing diogenites with basaltic eucrites. In addition, this diagram indicates that some polymict eucrites and one howardite appear to be dominated by Stannern-trend eucrites as their basaltic component. These meteorites plot above the main grouping of polymict breccias in Fig. 12b.

Petrographic study and siderophile element contents of HEDs provided early evidence for the presence of chondritic debris in howardites (e.g. Chou et al. 1976; Wilkening 1973). Systematic petrographic study has since shown that chondritic clasts, dominated by CM and to lesser extent CR materials, are present in many polymict breccias (Zolensky et al. 1996). Figure 12c shows Ni versus Mg for HED meteorites. The Ni contents of igneous lithologies are quite low. Warren et al. (2009) estimated Ni contents of 2.3 ± 2.8 μg/g for

pristine basaltic eucrites, 3.5 ± 3.0 μg/g for pristine cumulate eucrites, and 37 ± 36 μg/g for pristine diogenites. A 1% CM chondrite component would add 123 μg/g Ni to a polymict breccia. Excluding the three polymict breccias with > 900 μg/g Ni, howardites and polymict eucrites are estimated to contain 0–4% chondritic debris.

On average, howardites contain higher Ni contents than do polymict eucrites. Hewins (1982) noted that those howardites with higher Ni contents are also rich in solar wind-implanted noble gases. The higher Ni and solar wind gas contents suggest that the howardites were gardened on Vesta's surface, and thus they may be representative of the average material excavated by impacts. Warren et al. (2009) noted that the subset of howardites with high Ni and high solar wind gas contents show a limited range of Al contents of ~ 42–48 mg/g. They estimated that this corresponds to an approximate 2:1 mixture of eucrite:diogenite. Warren et al. (2009) suggested these howardites might represent ancient, well-mixed regolith. They refer to them as regolithic howardites to distinguish them from other howardites.

4 Chronology

Studies of radioactive isotopes and their daughter products in HEDs indicate a range of ages. These data constrain the timescale for Vesta's differentiation, the ages of its igneous crustal rocks, the chronology of its later impact history, and the duration of cosmic-ray exposure of HED meteorites in space. These ages provide a foundation for understanding Vesta's geologic evolution, and they can be compared with crater density ages estimated from Dawn imagery.

4.1 Age and Duration of Magmatic Activity

The timing of magmatism on Vesta can be constrained by determining the crystallization ages of its volcanic rocks. However, most HED meteorites have experienced thermal processing after crystallization (see below) and thus many radiochronometers record subsequent thermal events. Despite this complication, the ^{147}Sm-^{143}Nd ages of some basaltic eucrites indicate ancient magmatic activity close to ~ 4.56 Ga (e.g. Wadhwa and Lugmair 1995; Nyquist et al. 1997; Kumar et al. 1999). In some cases where the long-lived ^{147}Sm-^{143}Nd system has been reset, the short-lived ^{146}Sm-^{142}Nd system still indicates very early crystallization (Prinzhofer et al. 1992). Although the ^{87}Rb-^{87}Sr chronometer is more susceptible to thermal disturbance than the ^{147}Sm-^{143}Nd chronometer, the data for basaltic eucrites generally support ancient crystallization ages (e.g. Nyquist et al. 1986). The U-Pb system, the most precise method of absolute dating, in basaltic eucrites has generally been reset by later thermal events, but a ^{207}Pb-^{206}Pb isochron for the Asuka 881394 basaltic eucrite yields an age of 4566.5 ± 0.2 Ma (Wadhwa et al. 2009). Note, however, that this meteorite has an anomalous oxygen isotopic composition (Fig. 1) and other features, so its connection to Vesta is questionable (Scott et al. 2009a).

The former presence of short-lived radionuclides in basaltic eucrites supports their ancient ages. Excess ^{26}Mg formed by the decay of ^{26}Al in eucrite plagioclase (e.g. Srinivasan et al. 1999; Nyquist et al. 2003) suggests crystallization within ~ 5 Myr of the formation of the solar system (as defined by CAIs). The former presence of live ^{53}Mn has also been demonstrated in basaltic eucrites (Lugmair and Shukolyukov 1998; Nyquist et al. 2003, 2009; Trinquier et al. 2008). The ^{53}Mn-^{53}Cr ages indicate igneous activity began within

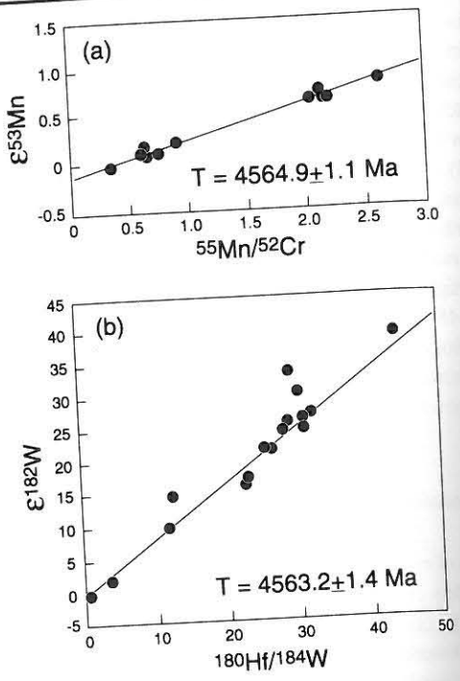

Fig. 13 Whole-rock isochrons used to determine the absolute age of the HED parent body. **a** ^{53}Mn-^{53}Cr systematics, after Trinquier et al. (2008). **b** ^{182}Hf-^{182}W systematics, after Wadhwa et al. (2006)

~ 3 Myr and continued until ~ 10 Myr after CAIs. Evidence for live ^{60}Fe in basaltic eucrites at the time of their crystallization (Shukolyukov and Lugmair 1993) also attests to early formation.

In contrast to the basaltic eucrites, the cumulate eucrites and diogenites have significant younger, concordant ^{147}Sm-^{143}Nd, ^{207}Pb-^{206}Pb, and sometimes ^{87}Rb-^{87}Sr ages (e.g. Jacobson and Wasserburg 1984; Takahashi and Masuda 1990; Tera et al. 1997). This later isotopic closure, as much as ~ 150 Myr after the basaltic eucrites, may imply that magmatism persisted for this long interval. Extended magmatism has also been suggested based on a 4430 ± 30 Ma ^{147}Sm-^{143}Nd age for the EET 90020 basaltic eucrite (Nyquist et al. 1997). It may be more likely, however, that slow cooling within the thermally insulated crust could account for the consistently younger ages of these plutonic rocks.

4.2 Timing of Global Differentiation

Internal mineral isochrons record ages of individual crustal rocks, whereas whole-rock isochrons (constructed with data from the entire HED group) reflect the timing of parent-daughter isotope fractionation in the mantle source—in other words, the age of differentiation to form the crust and mantle. A whole-rock ^{87}Rb-^{87}Sr isochron for the basaltic eucrites yields an age of 4.55 ± 0.6 Ga (Smoliar 1993). Whole-rock isochrons based on short-lived radionuclides define the timing of differentiation more precisely. The ^{53}Mn-^{53}Cr isochron for HEDs (Fig. 13a; Trinquier et al. 2008) gives a global silicate (crust-mantle) differentiation age of 2.2 ± 1.1 Myr after CAIs, corresponding to an absolute age of 4564.9 ± 1.1 Ma.

The ^{182}Hf-^{182}W chronometer defines the timing for core formation, because the short-lived hafnium isotope is lithophile and its tungsten decay product is siderophile. If metal fractionation occurred before ^{182}Hf had decayed, then the ratio of ^{182}W to non-radiogenic

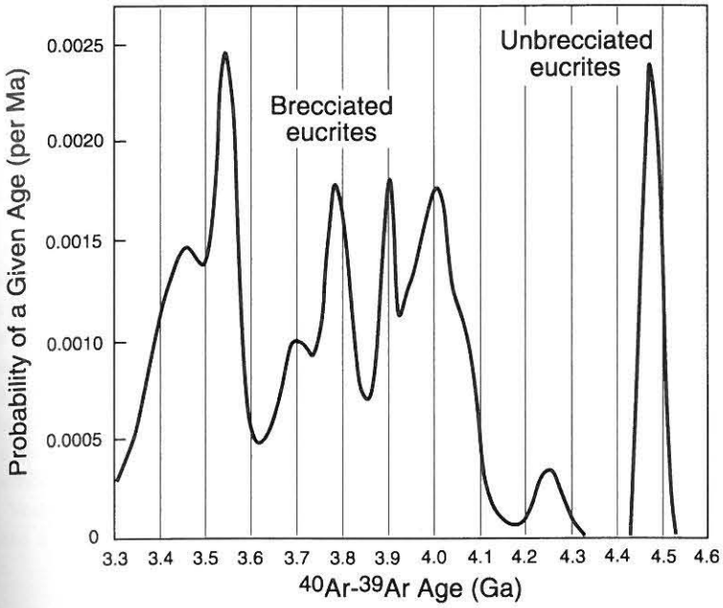

Fig. 14 Probability plot of ^{40}Ar-^{39}Ar ages of unbrecciated and brecciated eucrites, after Bogard and Garrison (2009). The peaks are thought to represent major impact events

^{184}W would be higher than chondritic in the silicate mantle, and consequently in the eucrites derived from it. Conversely, a lower ^{182}W/^{184}W would indicate later core formation. A whole-rock ^{182}Hf-^{182}W isochron for HEDs (Fig. 13b; Kleine et al. 2004 and Wadhwa et al. 2006) suggests that rapid core formation occurred 0.9 ± 0.3 Myr before silicate (crust-mantle) differentiation, at 4563.2 ± 1.4 Ma. However, Kleine et al. (2009) argued that the imprecisely defined isotopic ratios for average basaltic eucrites make the time of core formation more uncertain, and they calculated times of 3 ± 6 Myr after CAIs.

4.3 Thermal and Impact History

The timing of thermal and shock metamorphism is best determined from ^{40}Ar-^{39}Ar ages. Brecciated eucrites and howardites (near-surface samples) show evidence of significant Ar degassing, and their ^{40}Ar-^{39}Ar ages have been reset to between 4.1–3.4 Ga (Bogard and Garrison 2003). Some workers have argued that these ages represent thermal metamorphism on a global scale, and a model of pyroxene homogenization in eucrites by Miyamoto et al. (1985) suggested that such metamorphism occurred over an extended period of time (~ 1 Myr). However, the diffusion data in this model were uncertain. Bogard and Garrison (2009) have argued that the young ^{40}Ar-^{39}Ar ages represent impact events. Unbrecciated and unshocked eucrites have ages near 4.5 Ga, supporting the hypothesis that younger ages were reset by impacts. The ^{40}Ar-^{39}Ar ages of brecciated HEDs, illustrated on a Gaussian probability plot (Fig. 14; Bogard and Garrison 2009), mostly fall into clusters at ~ 4.0, 3.9, 3.8, and 3.5 Ga. The older ^{40}Ar-^{39}Ar ages overlap the period of the late heavy bombardment defined for the Moon. Could the Vestoids (and thus HEDs) have been excavated from the huge south pole impact basin at one of these times? Scott et al. (2009b) proposed that Vesta's

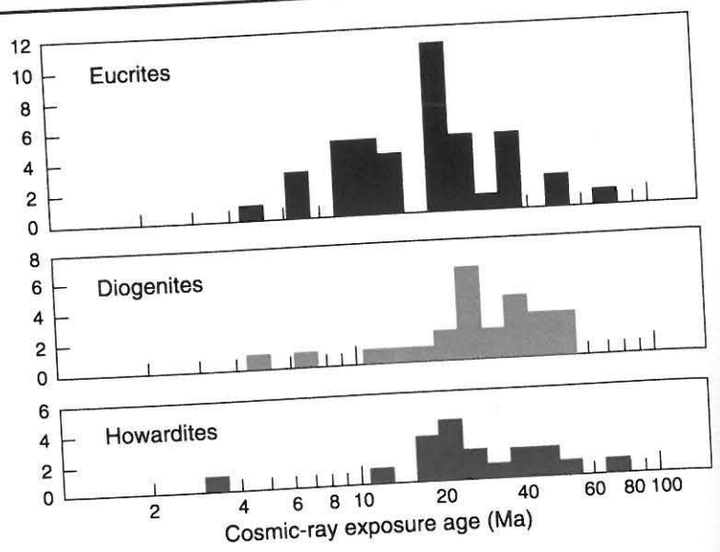

Fig. 15 Cosmic-ray exposure ages for HED meteorites, after Eugster et al. (2006)

large south pole crater may have been formed during the later 3.5 Ga event. This age is later than the late heavy bombardment, and simulations of the orbital evolution of main belt asteroids suggest that if the Vestoids had formed before the late heavy bombardment, their orbits would be more scattered than presently observed (Gomes et al. 2005). However, Marzari et al. (1996) proposed an upper bound of ~ 1 Ga for the formation of the Vestoids, based on orbital and collisional dynamics. Binzel et al. (1997) also suggested a fairly young age for Vestoids, based on their spectral characteristics.

4.4 Sampling and Cosmic-Ray Exposure

Cosmic-ray exposure ages for HED meteorites have been summarized by Eugster and Michel (1995), Welten et al. (1997), and Eugster et al. (2006). Basaltic and cumulate eucrites, diogenites, and howardites all form clusters at ~ 22 and ~ 36 Myr, and an additional eucrite-only cluster occurs at ~ 12 Myr (Fig. 15). These ages are much younger than the ^{40}Ar-^{39}Ar ages for HEDs. This may imply that cosmic-ray exposure, which dates the orbital lifetimes of sub-meter size meteors, was initiated by impacts into Vestoids (Binzel and Xu 1993); if correct, multi-km size Vestoids must contain all three members of the HEDs. Alternatively, these ages could reflect derivation by recent impacts on Vesta itself, because the 10–40 Ma cosmic-ray ages are consistent with orbital evolution from Vesta by the Yarkovsky effect (Bottke et al. 2000).

The circled data shown in Fig. 12 are HED meteorites that fall within the ~ 22 Ma exposure age peak. These meteorites include representatives of both basaltic eucrite chemical trends, cumulate eucrites, diogenites, polymict eucrites and howardites. Were all these meteorites having the same cosmic-ray exposure age sampled by the same cratering event? Eugster and Michel (1995) interpreted the cosmic-ray exposure age histogram as showing that five such impact events are represented, suggesting that the surface of the parent asteroid may be well sampled.

5 Implications of HEDs for Vesta's Geologic History

A goal of the Dawn mission is to provide data needed to construct an integrated geologic history of Vesta. That history should be consistent with what is inferred from HED meteorites.

5.1 Timing and Location of Vesta's Formation

Vesta's accretion cannot be dated directly but its time of differentiation, no more than 1–3 Myr after CAIs, as determined from HEDs, indicates that its formation was early. A previous report that Vesta formed before ^{60}Fe (produced in a supernova) was injected into the solar nebula (Bizzarro et al. 2007), based on analyses of HEDs, has now been refuted (Dauphas et al. 2008).

Bottke et al. (2005) suggested that differentiated asteroids, such as Vesta, formed in the terrestrial planet region, rather than at their present heliocentric distances. Earlier accretion is expected closer to the Sun, where the swarm density of particles was higher, and early-formed planetesimals would have incorporated more live ^{26}Al to facilitate melting. If correct, Vesta could be viewed as an unused planetary building block that escaped incorporation into a terrestrial planet and was later perturbed into an orbit at greater heliocentric distance.

5.2 Bulk Composition of Vesta

The basaltic eucrites and howardites provide indirect evidence for the bulk compositional characteristics of Vesta (Consolmagno and Drake 1977; Dreibus and Wänke 1980; Mittlefehldt 1987; Morgan et al. 1978). Common features of model bulk compositions are low alkali element contents, but refractory lithophile element contents near chondritic abundances.

The Na and Al contents of eucrites are almost entirely contained in plagioclase. Melting experiments (Stolper 1977) and REE modeling (Consolmagno and Drake 1977) show that the most primitive basaltic eucrite compositions were not in equilibrium with plagioclase. Thus, plagioclase was not a solid phase on the HED parent asteroid when primitive basaltic eucrites formed, and their Na/Al ratios will be close to that of the bulk asteroid regardless of the formation mechanism (partial melting or fractional crystallization). Sodium was a moderately volatile element during condensation of the nebular gas, while Al was refractory (e.g. Lodders 2003). The Na/Al of basaltic eucrites is then a representative fingerprint of the moderately volatile element fractionation recorded in the material that accreted to form Vesta.

Ferrous Fe and Mn^{2+} are homologous species. Their ionic radii differ by only ~ 6% and therefore ferromagnesian phases do not greatly fractionate MnO from FeO during igneous processes. The FeO/MnO of Vesta is expected to be close to that of basaltic eucrites (Dreibus and Wänke 1980). Iron condensed as metal in the solar nebula, and reactions with the cooling gas converted some of the metal to FeS and the FeO component of ferromagnesian silicates (Lodders 2003). Thus, the FeO content of silicates is related to the degree of oxidation of the initial nebular condensates. Manganese condenses as a component in olivine and pyroxene at a temperature ~ 180° below the condensation temperature of Fe metal, but well above the temperature where oxidation occurs (Lodders 2003). Volatility-controlled nebular fractionation of Mn from total Fe may also have occurred. Nevertheless, the FeO/MnO ratio of eucrites serves as a general indicator of Vesta's oxidation state.

Figure 16 shows molar Na/Al versus FeO/MnO for basaltic eucrites compared to different chondrite types, another group of asteroidal basalts (angrites), and two ungrouped

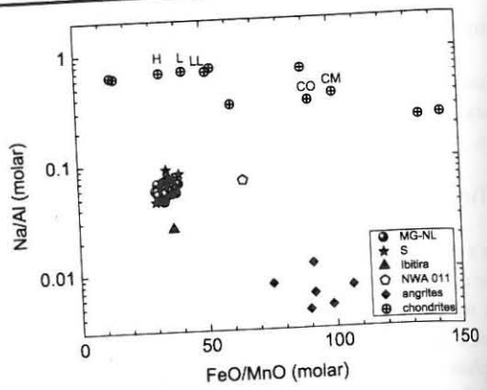

Fig. 16 Molar Na/Al vs. FeO/MnO for asteroidal basalts compared to average bulk chondrites from Lodders and Fegley (1998). For the chondrite averages, bulk Fe was apportioned between metal, sulfides, silicates and magnetite to estimate silicate FeO/MnO

basaltic achondrites (Ibitira and NWA 011). The HED parent asteroid is moderately reduced, with an FeO/MnO ratio similar to that of ordinary chondrites. This agrees well with what is known about the oxygen fugacities of HEDs and ordinary chondrites. Measurements of the intrinsic oxygen fugacity of ordinary chondrites yield a range of values from ~ 0.4 to 1.1 log units below the iron-wüstite buffer (IW) (Brett and Sato 1984). Stolper (1977) inferred an oxygen fugacity for eucrite petrogenesis via partial melting of ~ 1 log unit below IW, and Hewins and Ulmer (1984) measured the intrinsic oxygen fugacity of two diogenites to be at or ~ 0.5 log units above IW. Ibitira has a FeO/MnO ratio close to those of basaltic eucrites, whereas NWA 011 has a much higher ratio, suggesting a more oxidized parent body. The angrites have the highest FeO/MnO ratios among asteroidal basalts, indicating a parent asteroid with an oxidation state similar to that of CO or CM chondrites.

The Na/Al ratio of eucrites is substantially lower than that of any chondrite type. The Na/Al ratios of CV and CK chondrites are about a factor of 3 higher than measured for Stannern-trend eucrites (~ 0.07–0.09). The low Na/Al ratios for basaltic eucrites indicate a factor of 10 depletion in Na for 4 Vesta when compared to solar abundances. Even greater depletions in the other alkali elements, up to a factor of ~ 250 for Cs, were estimated by Mittlefehldt (1987). NWA 011 has a Na/Al ratio like those of basaltic eucrites, suggesting similar moderately volatile element depletions for its parent asteroid, but the Na/Al ratio of Ibitira is less than half that of basaltic eucrites. Angrites are severely depleted in moderately volatile elements, with Na/Al ratios roughly an order of magnitude lower than those of basaltic eucrites. Depletion in moderately volatile and highly volatile elements appears characteristic of many differentiated asteroids like Vesta.

Other constraints suggest that Vesta's bulk chemical composition was chondritic. The REE patterns for eucrites can be modeled from a chondritic source (Consolmagno and Drake 1977), and the narrow range in Sm/Nd and Lu/Hf ratios among eucrites suggest they formed as large-degree melts from a source having chondritic abundances of refractory lithophile elements (Blichert et al. 2002). As already noted, however, it is not possible to reconcile the low alkali element abundances in eucrites with known chondrite compositions.

The compositions of primary magmas can be used to constrain their mantle source region compositions, provided adequate assumptions about the degree of partial melting can be made. Stolper (1977) hypothesized that some eucrites were primary melts, but other workers (e.g. Takeda 1997; Warren 1985) have argued that primitive liquid compositions are absent from the HED collection. Melting experiments (Jurewicz et al. 1993, 1995) using carbonaceous and ordinary chondrites demonstrated that partial melts of CM chondrites had compositions similar to eucrites, so long as volatiles could have escaped the system

However, the CM chondrite experimental melts could not produce enough orthopyroxene to explain the occurrence of diogenite cumulates (Jurewicz et al. 1993). LL chondrite melts produced orthopyroxene in abundance, but these melts were unlike eucrites (Jurewicz et al. 1995). Righter and Drake (1997) favored a mixture of CM and L chondrites that satisfied the oxygen isotopes, the FeO/MnO ratio, and siderophile and lithophile trace element abundances for eucrites.

If Vesta differentiated via near-total melting and fractional crystallization (Ruzicka et al. 1997; Warren 1997) as discussed below, then eucrites are not direct probes of the mantle of the parent asteroid. In that case, parent body models that rely on the assumption of equilibrium between melt and mantle (e.g. Consolmagno and Drake 1977; Jones 1984) are invalid. The constraints derived from Na/Al and FeO/MnO above are still valid, though, and Fig. 16 remains useful for estimating the moderately volatile element depletion and relative oxidation state of Vesta.

5.3 Global Differentiation of Vesta

Haack et al. (1990) devised a thermal evolution models for Vesta based on long-lived radionuclide decay. However, the recognition that the HED parent body accreted very early means that it incorporated significant quantities of short-lived radionuclides like ^{26}Al and ^{60}Fe, which would have dominated its early thermal history. The thermal model of Ghosh and McSween (1998), based on short-lived radionuclide heating and constrained by the properties of HEDs, divided Vesta's evolution into stages: (1) radiogenic heating of a homogeneous asteroid until metal-sulfide eutectic melting and core separation; (2) further heating of the mantle until silicate partial melting and crust formation; and (3) subsequent heating and cooling of the differentiated body. Thermal calculations for Vesta are complicated due to the migration of heat sources during the simulation (^{60}Fe is incorporated into the core and ^{26}Al into the crust). The model produced a reverse geothermal gradient, which minimized heat loss from the asteroid's interior for ~ 100 Myr.

Short-lived radionuclides in HEDs suggest that Vesta's core separated ~ 1 Myr before mantle melting was extensive enough to form the crust (Kleine et al. 2004; Wadhwa et al. 2006), consistent with the model above and with the observation that the eucrite source region was demonstrably metal-free (Righter and Drake 1997). The crystallization ages of basaltic eucrites indicate volcanism extended for ~ 10 Myr and possibly longer (Trinquier et al. 2008). Older radiometric ages for rocks formed deeper in the crust (cumulate eucrites and diogenites) may suggest that magmatism continued for perhaps another 100 Myr, or these younger ages may simply reflect slow cooling to isotope blocking temperatures.

Although some geochemical evidence appears to favor crystallization of a largely molten asteroid as the operative mechanism for formation of the HED igneous suite, this leaves unexplained the experimental observation that those basaltic eucrites with the most primitive compositions (highest mg#, lowest Sc, Ti, Hf) are saturated with olivine on their liquidi, indicating equilibration with olivine in the source region (Stolper 1977). This is an unlikely result if a magma ocean underwent fractional crystallization. Modeling of this process shows that there is an extended period of crystallization of orthopyroxene ± chromite between the cessation of olivine crystallization and the point where the melt becomes saturated in plagioclase (i.e. becomes eucritic) (Ruzicka et al. 1997). Nevertheless, Warren (1985) developed a schematic scenario that purportedly can explain olivine saturation on the liquidus of residual melts.

Equilibrium crystallization of a magma ocean is an alternative mechanism (Righter and Drake 1997). This process can explain Stolper's result because equilibrium crystallization

is thermodynamically equivalent to equilibrium partial melting run in reverse. The model considers that convective mixing of the magma is efficient during the period of olivine, orthopyroxene, and chromite crystallization, but becomes "locked" at the point when the residual melt has the composition of main-group eucrites. From then on, fractional crystallization forms Nuevo Laredo-trend eucrites (Righter and Drake 1997). Although this model can reconcile Stolper's observation with the compositional constraints discussed earlier it appears to contradict petrologic observations of diogenites. The model would predict an intimate mixture of olivine, orthopyroxene, and chromite as the crystalline phases at the point of convective lock-up, with olivine being the dominant phase (Righter and Drake 1997). This contrasts sharply with modal abundance measurements that show that olivine is absent or a minor phase in most diogenites (Bowman et al. 1997).

Basaltic eucrites have a narrow range of Cr contents, and this has also been cited as evidence against magma ocean crystallization models (Jurewicz et al. 1993). Stolper (1977) found that basaltic eucrites are saturated with Cr-rich spinel on their liquidi, and concluded that spinel was a residual phase in the source region. Residual Cr-rich spinel would buffer the Cr content of primary partial melts to yield a narrow range of values. This is consistent with basaltic eucrite data—50% of basaltic eucrites have Cr contents of 2.1 ± 0.1 mg/g. The average Cr contents of spinel-saturated experimental melts from Murchison and Allende run at eucrite conditions is 2.1 mg/g (Jurewicz et al. 1993). These authors argued that because Cr is a compatible element in pyroxene, formation of eucrites as residual melts after diogenite formation is unlikely to have resulted in Cr-spinel saturated magmas.

Magma ocean crystallization models in their simplest form imply that there was a single liquid line of decent, whereas the compositional evidence from basaltic eucrites shows two or more crystallization trends (Fig. 8b). The distinction between main-group–Nuevo Laredo-trend eucrites and Stannern-trend eucrites in particular is difficult to understand in the context of whole-asteroid crystallization (Mittlefehldt and Lindstrom 2003). A recent model posits that Stannern-trend eucrites were formed by partial assimilation of earlier basalts by magmas rising through the nascent Vestan crust (Barrat et al. 2007). This hypothesis holds promise, but requires testing. Serial tapping of the residual melt from whole-asteroid crystallization has been suggested as a mechanism for forming eucrite compositional suites (Warren 1997) and for engendering the pervasive metamorphism of eucritic basalts (Yamaguchi et al. 1996). Also, trace element data for diogenites demonstrate that they cannot all have formed from a common magma (Mittlefehldt 1994; Barrat et al. 2008), as would be expected for a magma ocean model. However, producing diogenites in multiple plutons either requires ultramafic magmas or significant quantities of complementary gabbro, samples of which have not been recognized among the HEDs.

5.4 Compositions, Proportions and Densities of Vesta's Core, Mantle and Crust

Siderophile element depletions in HEDs, relative to chondrites, provide evidence for a metallic FeNi core in the parent body (Hewins and Newsom 1988; Righter and Drake 1997). Preferred estimates of the mass of the core vary between 5–25% (Righter and Drake 1997) based on models of siderophile element abundances in chondrites, and between 4–30% (Ruzicka et al. 1997) based on mixtures of HED minerals that produce chondritic element ratios. The bulk density used in the calculation of Ruzicka et al. (1997) was ~ 3.54 g/cm^3, lower than the ~ 3.76 g/cm^3 value calculated from the most recent Vesta mass determination (Konopliv et al. 2006) and HST diameter measurements (Thomas et al. 1997). The higher bulk density indicates that the core mass is greater than the lower bounds of the previous estimates.

Although orthopyroxene is the dominant mineral in diogenites, the occurrence of a limited number of olivine-bearing diogenites and a dunite having HED oxygen isotopic composition suggest that olivine may be a significant component of the mantle. In addition, a region on Vesta shows a spectrum interpreted to show olivine, suggesting a crater may have excavated dunite below an orthopyroxenite layer (Gaffey 1997). The normative mineralogies of modeled bulk-silicate (mantle + crust) compositions for the HED parent body (Dreibus and Wänke 1980; Jones 1984) contain $\sim$ 50–75% olivine, with 16–42% pyroxene and 9–10% plagioclase (Ruzicka et al. 1997). The bulk-silicate densities of these mineral assemblages are 3.42–3.63 g/cm^3.

The crust is acknowledged to be basaltic in composition, but it must contain a significant fraction of ultramafic cumulates (diogenite). The chemical compositions of regolith howardites correspond a eucrite:diogenite mixing ratio of 2:1 (Warren et al. 2009). The normative mineralogy of that composition is $\sim$ 70% pyroxene and 25% plagioclase, corresponding to a density of 3.17 g/cm^3. However, Warren et al. (2009) suggest that this ratio is an upper limit, and the real crustal proportions may be closer to 1:1 because of bias in the impact sampling of deeper lithologies. The volume of the crust is not well constrained. Miyamoto and Takeda (1994) estimated a minimum thickness of $\sim$ 8 km, based on a model of cooling and exsolution of pyroxene in a cumulate eucrite. This estimate is consistent with the size of the largest Vestoid with eucrite-like spectra (diameter of $\leq$ 10 km, Binzel and Xu 1993). Ruzicka et al. (1997) estimated a 24–41 km-thick eucritic crust, assuming that the bulk asteroid had an Al_2O_3 abundance greater than chondritic. A chondritic bulk asteroid would have a crust $\sim$ 19 km thick.

5.5 Thermal and Impact History of Vesta

Most HED meteorites have experienced thermal metamorphism. Takeda et al. (1997) argued that impacts into a hot crust could account for global metamorphism. Baking of eucrite flows by heat from later, superjacent flows (Warren 1997) or from underlying plutons that produced a steep thermal gradient in the crust (Yamaguchi et al. 1996) have also been proposed. However, cooling rates calculated for thermal relaxation of the deep crust are much slower than those estimated from pyroxene exsolution in metamorphosed eucrites (Schwartz and McCallum 2005), suggesting that they cooled in thick ejecta blankets.

Vesta experienced major impacts between 4.1 and 3.5 Ga, as recorded by ^{40}Ar-^{39}Ar shock ages of HEDs (Bogard and Garrison 2009). It is unclear whether one such collision produced the Vestoids (and HEDs) from the south pole crater, or whether the Vestoids were excavated from that crater much later. Impacts produced breccias composed of eucrite and diogenite fragments in varying proportions. Although a few exotic clasts appear in howardites, their scarcity suggests that the HED breccias may provide a representative sampling of Vesta's crust.

The magnetic anisotropy measurements on HEDs imply deformation after the last brecciation events (Gattecceca et al. 2008). It is unclear whether the magnetic field was internally generated, in which case the core must have been partly molten for a considerable period, or was generated through hypervelocity impacts.

Clusters of cosmic-ray exposure ages that contain all the HED rock types might implicate large impacts that sampled Vesta's vertical stratigraphy. However, these ages are significantly younger than ^{40}Ar-^{39}Ar ages and may reflect impacts into Vestoids or V-class near-Earth asteroids that liberated individual HEDs.

5.6 Regolith Formation on Vesta

Judging from spectroscopic observations that suggest portions of Vesta's surface are dominated by eucrite or diogenite (Binzel et al. 1997; Gaffey 1997), it would appear that impacts have not produced a globally homogenized regolith covering the surface. Warren et al. (2009), however, suggested that the heterogeneous surface is a modification, late in the asteroid's history, caused by ejecta from the south pole impact (they do not accept an ancient age for this basin). Based on petrographic differences among HED polymict breccias, Saiki and Takeda (1999) suggested that the parent body is heterogeneous on local scales and that most breccias formed in the proximity of impact craters. Several other observations support the idea that the regolith is not as well developed, as processed, or as homogenized as on the Moon. Howardites are less "mature" than lunar regolith samples, as indicated by the scarcity of agglutinates and grains with solar-flare tracks (Caffee et al. 1988). Also, only a minor portion of HED polymict breccias contain implanted solar wind gases (Bischoff et al. 2006; Warren et al. 2009) and are thus true regolith samples, implying that gardening has not been extensive. The higher cratering rate in the asteroid belt is expected to have caused rapid turnover of surface materials (Housen and Wilkening 1982), perhaps preventing a significant portion of HED polymict breccias from becoming gas-rich.

6 Implications of HEDs for the Dawn Mission

HEDs provide a detailed geologic framework, summarized in Sect. 5, for Dawn's exploration of Vesta. It is instructive to compare the exploration of Vesta with that of the Moon. Before obtaining lunar samples, geologic maps of the Moon had already been made and a stratigraphic (relative-time) framework was in place. Lunar samples subsequently returned by the Apollo astronauts revolutionized interpretations of the Moon's formation and geologic history, provided geochemical ground truth for orbital remote-sensing, and established an absolute timescale for crater-counting chronology. For Vesta, we have the opposite situation—we already have a large collection of samples in hand, but without geologic context. From HEDs we understand a great deal about Vesta's differentiation, magmatic and impact history, and chronology. But observations of the body itself, from Earth-based telescopes and the Hubble Space Telescope, provide only hazy glimpses into its geologic and compositional complexities.

Besides providing a working geologic framework with which the interpretations of Dawn's data should accord, how will HEDs influence the exploration of Vesta? Knowledge of HED mineralogy will complement mineral identifications by Dawn's VIR and FC spectrometers. The laboratory spectra of eucrites (Mayne et al. 2010) and diogenites (Burbine et al. 2001) having known mineral proportions and compositions can aid in identifying the petrologic units to be mapped on Vesta, as well as quantifying the mixing proportions of eucrite and diogenite in howardite terranes. The characteristics of diogenites containing olivine (Beck and McSween 2010) may be important in interpreting spectra of olivine-bearing materials exposed within the south pole crater and elsewhere (Binzel et al. 1997; Gaffey 1997). A knowledge of olivine compositions—both those measured in diogenites and predicted from melting and crystallization models—should allow the determination of the origin of any olivine-bearing rocks exposed in the crater. HEDs also provide some constraints on the thickness of the crust (Miyamoto and Takeda 1994; Ruzicka et al. 1997) and size of the core (Righter and Drake 1997) that might be tested with images of large craters and gravity science from spacecraft tracking. The chemical compositions of HEDs

can also constrain the mixing ratios of eucrite and diogenite in the large areas to be chemically analyzed by GRaND (Usui and McSween 2007). The discovery of small amounts of exotic materials such as carbonaceous chondrite clasts (Gounelle et al. 2003), K-rich impact glasses (Barrat et al. 2009), and Fe-rich, highly differentiated clasts (Ikeda and Takeda 1985) in howardite breccias suggest possible target materials that might be detected spectroscopically or chemically from orbit. HED chronology may allow crater densities on Vesta to be calibrated, and chronological and bulk compositional constraints from HEDs are essential for the construction of more rigorous thermal evolution models.

Working backward, from samples to orbital observations and measurements, may prove as challenging as working forward was for the Moon, but without HEDs the exploration of Vesta by the Dawn spacecraft would not be nearly so revealing.

Acknowledgements We acknowledge thoughtful reviews by P. Warren and an anonymous reviewer. This work was partly supported by NASA Cosmochemistry grants NNG06GG36G (HYM), RTOP 344-31-10-18 (DWM), and NNG06GF56G (TJM).

References

J.A. Barrat, A. Yamaguchi, R.C. Greenwood, M. Bohn, J. Cotton, M. Benoit, I.A. Franchi, Geochim. Cosmochim. Acta **71**, 4108 (2007)
J.A. Barrat, A. Yamaguchi, M. Benoit, J. Cotton, M. Bohn, Meteorit. Planet. Sci. **43**, 1759 (2008)
J.A. Barrat, M. Bohn, Ph. Gillet, A. Yamaguchi, Meteorit. Planet. Sci. **44**, 359 (2009)
A.W. Beck, H.Y. McSween, Lunar Planet. Sci. **XXXIX**, CD #1391 (2008)
A.W. Beck, H.Y. McSween, Meteorit. Planet. Sci. (2010, in press)
J.L. Berkley, N.J. Boynton, Meteoritics **27**, 387 (1992)
A. Bischoff, E.R.D. Scott, K. Metzler, C.A. Goodrich, in *Meteorites and the Early Solar System II*, ed. by D.S. Lauretta, H.Y. McSween (University of Arizona Press, Tucson, 2006), p. 679
R.P. Binzel, S. Xu, Science **260**, 186 (1993)
R.P. Binzel, M.J. Gaffey, P.C. Thomas, B.H. Zellner, A.D. Storrs, E.N. Wells, Icarus **128**, 95 (1997)
M. Bizzarro, D. Ulfbeck, A. Trinquier, K. Thrane, J.N. Connelly, B.S. Meyer, Science **316**, 1178 (2007)
J. Blichert, M. Boyet, P. Telouk, F. Albarede, Earth Planet. Sci. Lett. **204**, 167 (2002)
D.D. Bogard, D.H. Garrison, Meteorit. Planet. Sci. **38**, 669 (2003)
D.D. Bogard, D.H. Garrison, Lunar Planet. Sci. **XL**, CD #1131 (2009)
W.F. Bottke, D.P. Rubincam, J.A. Burns, Icarus **145**, 301 (2000)
W.F. Bottke, D. Nesvorny, R.E. Grimm, A. Morbidelli, D.P. O'Brien, Nature **439**, 821 (2005)
L.E. Bowman, M.N. Spilde, J.J. Papike, Meteorit. Planet. Sci. **32**, 869 (1997)
L.E. Bowman, J.J. Papike, M.N. Spilde, Am. Mineral. **84**, 1020 (1999)
R. Brett, M. Sato, Geochim. Cosmochim. Acta **48**, 111 (1984)
P.C. Buchanan, D.J. Lindstrom, D.W. Mittlefehldt, C. Koeberl, W.U. Reimold, Meteorit. Planet. Sci. **35**, 1321 (2000)
P.C. Buchanan, M.E. Zolensky, R.C. Greenwood, I.A. Franchi, Meteorit. Planet. Sci. **44**, A42 (2009)
T.H. Burbine, P.C. Buchanan, R.P. Binzel, S.J. Bus, T. Hiroi, J.L. Hinrichs, A. Meibom, T.J. McCoy, Meteorit. Planet. Sci. **36**, 761 (2001)
T.E. Bunch, Proc. Lunar Sci. Conf. **6**, 469 (1975)
T.E. Bunch, R.S. Rajan, in *Meteorites and the Early Solar System*, ed. by J.F. Kerridge, M.S. Matthews (University of Arizona Press, Tucson, 1988), p. 144
M.W. Caffee, J.N. Goswami, C.M. Hohenburg, K. Marti, R.C. Reedy, in *Meteorites and the Early Solar System*, ed. by J.F. Kerridge, M.S. Matthews (University of Arizona Press, Tucson, 1988), p. 205
H. Chennaoui Aoudjehanne, A. Jambon, Lunar Planet. Sci. **XXXVIII**, CD #1714 (2007)
C.-L. Chou, W.V. Boynton, R.W. Bild, J. Kimberlin, J.T. Wasson, Proc. Lunar Sci. Conf. **7**, 3501 (1976)
D.W. Collinson, S.J. Morden, Earth Planet. Sci. Lett. **126**, 421 (1994)
G.Y. Consolmagno, M.J. Drake, Geochim. Cosmochim. Acta **41**, 1271 (1977)
D.P. Cruickshank, D.J. Tholen, W.K. Hartmann, J.F. Bell, R.H. Brown, Icarus **89**, 1 (1991)
N. Dauphas, D.L. Cook, A. Sacarabany, C. Frohlich, A.M. Davis, M. Wadhwa, A. Pournand, T. Rauscher, R. Gallino, Astrophys. J. **686**, 560 (2008)
J.S. Delaney, M. Prinz, C.E. Nehru, G.E. Harlow, Lunar Planet. Sci. **XII**, 211 (1981)

J.S. Delaney, H. Takeda, M. Prinz, C.E. Nehru, G.E. Harlow, Meteoritics **18**, 103 (1983)
J.S. Delaney, M. Prinz, H. Takeda, J. Geophys. Res. **89**, C251 (1984)
K. Domanik, S. Kolar, D. Musselwhite, M.J. Drake, Meteorit. Planet. Sci. **39**, 567 (2004)
M.C. Domeneghetti, G.M. Molin, M. Stimpfl, M. Tribaudino, Am. Mineral. **80**, 923 (1995)
G. Dreibus, H. Wänke, Z. Naturforsch. **35a**, 204 (1980)
O. Eugster, T. Michel, Geochim. Cosmochim. Acta **59**, 177 (1995)
O. Eugster, G.F. Herzog, K. Marti, M.W. Caffee, in *Meteorites and the Early Solar System II*, ed. by D.S. Lauretta, H.Y. McSween (University of Arizona Press, Tucson, 2006), p. 829
R.J. Floran, M. Prinz, P.F. Hlava, K. Keil, B. Spettel, H. Wänke, Geochim. Cosmochim. Acta **45**, 2385 (1981)
G.W. Fowler, J.J. Papike, M.N. Spilde, C.K. Shearer, Geochim. Cosmochim. Acta **58**, 3921 (1994)
G.W. Fowler, C.K. Shearer, J.J. Papike, G.D. Layne, Geochim. Cosmochim. Acta **59**, 3071 (1995)
M.J. Gaffey, Icarus **127**, 130 (1997)
J. Gattecceca, P. Rochette, M. Gounelle, M. Van Gilleken, Earth Planet. Sci. Lett. **270**, 280 (2008)
A. Ghosh, H.Y. McSween, Icarus **134**, 187 (1998)
R. Gomes, H.F. Levison, K. Tsiganis, A. Morbedelli, Nature **435**, 466 (2005)
R. Gooley, C.B. Moore, Am. Mineral. **61**, 373 (1976)
M. Gounelle, M.E. Zolensky, J.-C. Liou, P.A. Bland, O. Alard, Geochim. Cosmochim. Acta **67**, 507 (2003)
R.C. Greenwood, I.A. Franchi, A. Jambon, P.C. Buchanan, Nature **435**, 916 (2005)
R.C. Greenwood, I.A. Franchi, A. Jambon, J.A. Barrat, T.H. Burbine, Science **313**, 1763 (2006)
H. Haack, K.L. Rasmussen, P.H. Warren, J. Geophys. Res. **95**, 5111 (1990)
T.A. Harriott, R.H. Hewins, Meteoritics **19**, 15 (1984)
R.H. Hewins, in *Workshop on Lunar Breccias and Soils and Their Meteoritic Analogs*, ed. by G.J. Taylor, L.L. Wilkening (Lunar and Planetary Institute, Houston, 1982), p. 44
R.H. Hewins, H.E. Newsom, in *Meteorites and the Early Solar System*, ed. by J.F. Kerridge, M.S. Matthews (University of Arizona Press, Tucson, 1988), p. 73
R.H. Hewins, G.C. Ulmer, Geochim. Cosmochim. Acta **48**, 1555 (1984)
A. Holzheid, H. Palme, Meteorit. Planet. Sci. **42**, 1817 (2007)
K.R. Housen, L.L. Wilkening, Annu. Rev. Earth Planet. Sci. **10**, 355 (1982)
W. Hsu, G. Crozaz, Geochim. Cosmochim. Acta **60**, 4571 (1996)
Y. Ikeda, H. Takeda, J. Geophys. Res. **90**, C649 (1985)
A.J. Irving, S.M. Kuehner, D. Rumble, A.C. Hupé, G.M. Hupé, Lunar Planet. Sci. **XXXIV**, CD #1502 (2003)
S.B. Jacobson, G.J. Wasserburg, Earth Planet. Sci. Lett. **67**, 137 (1984)
J.H. Jones, Geochim. Cosmochim. Acta **48**, 641 (1984)
J.H. Jones, in *A Handbook of Physical Constants: Rock Physics and Phase Relations*, ed. by T.J. Ahrens (Am. Geophys. Union, Washington, 1995), p. 73
A.J.G. Jurewicz, D.W. Mittlefehldt, J.H. Jones, Geochim. Cosmochim. Acta **57**, 2123 (1993)
A.J.G. Jurewicz, D.W. Mittlefehldt, J.H. Jones, Geochim. Cosmochim. Acta **59**, 391 (1995)
K. Keil, in *Asteroids III*, ed. by W. Bottke, A. Cellino, P. Paolicchi, R.P. Binzel (University of Arizona Press, Tucson, 2002), p. 573
T. Kleine, K. Mezger, C. Munker, H. Palme, A. Bischoff, Geochim. Cosmochim. Acta **68**, 2935 (2004)
T. Kleine, M. Touboul, B. Bourdon, F. Nimmo, K. Mezger, H. Palme, S.B. Jacobsen, Q.-Z. Yin, A.N. Halliday, Geochim. Cosmochim. Acta **73**, 5150 (2009)
A.S. Konopliv, C.F. Yoder, E.M. Standish, D.-N. Yuan, W.L. Sjogren, Icarus **182**, 23 (2006)
M.J. Krawczynski, L.T. Elkins-Tanton, T.L. Grove, Lunar Planet. Sci. **XXXIX**, CD #1229 (2008)
A. Kumar, K. Gopalan, N. Bhandari, Geochim. Cosmochim. Acta **63**, 3997 (1999)
D. Lazzaro, T. Michtchenko, J.M. Carvano, R.P. Binzel, S.J. Bus, T.H. Burbine, T. Mothe-Dinz, M. Florczak, C.A. Angeli, A.W. Harris, Science **288**, 2033 (2000)
M.M. Lindstrom, D.W. Mittlefehldt, Meteoritics **27**, 250 (1992)
K. Lodders, Astrophys. J. **591**, 1220 (2003)
K. Lodders, B. Fegley Jr., *The Planetary Scientists' Companion* (Oxford Univ. Press, New York, 1998) 371 pp.
G.W. Lugmair, A. Shukolyukov, Geochim. Cosmochim. Acta **62**, 2863 (1998)
F. Marzari, A. Cellino, D.R. Davis, P. Farinella, V. Zappala, V. Vanzani, Astron. Astrophys. **316**, 248 (1996)
B. Mason, *Meteorites* (Wiley, New York, 1962), 274pp.
B. Mason, in *Extra-Terrestrial Matter*, ed. by C.A. Randall Jr. (Northern Illinois University Press, DeKalb, 1969), p. 3
B. Mason, Am. Mus. Novit. **2155**, 13 (1963)
R.G. Mayne, H.Y. McSween, T.J. McCoy, A. Gale, Geochim. Cosmochim. Acta **73**, 794 (2009)
R.G. Mayne, J.M. Sunshine, H.Y. McSween, T.J. McCoy, C.M. Corrigan, A. Gale, M.D. Dyar, Meteorit. Planet. Sci. (2010, in press)
T.B. McCord, J.B. Adams, T.V. Johnson, Science **168**, 1445 (1970)

T.J. McCoy, R.A. Ketcham, L. Wilson, G.K. Benedix, M. Wadhwa, A.M. Davis, Earth Planet. Sci. Lett. **246**, 102 (2006)
D.W. Mittlefehldt, Geochim. Cosmochim. Acta **51**, 267 (1987)
D.W. Mittlefehldt, Geochim. Cosmochim. Acta **58**, 1537 (1994)
D.W. Mittlefehldt, Meteorit. Planet. Sci. **35**, 901 (2000)
D.W. Mittlefehldt, Meteorit. Planet. Sci. **40**, 665 (2005)
D.W. Mittlefehldt, Lunar Planet. Sci. **XXXIX**, CD #1919 (2008)
D.W. Mittlefehldt, M.M. Lindstrom, in *Proc. NIPR Symp. Antarctic Met.*, vol. 6 (1993), p. 268
D.W. Mittlefehldt, M.M. Lindstrom, Geochim. Cosmochim. Acta **61**, 453 (1997)
D.W. Mittlefehldt, M.M. Lindstrom, Geochim. Cosmochim. Acta **67**, 1911 (2003)
D.W. Mittlefehldt, T.J. McCoy, C.A. Goodrich, A. Kracher, in *Planetary Materials, Reviews in Mineralogy*, ed. by J.J. Papike, vol. 36 (Mineral. Soc. Am., Washington, 1998), p. 195
D.W. Mittlefehldt, A.W. Beck, C.-T.A. Lee, H.Y. McSween, Lunar Planet. Sci. **XL**, CD #1038 (2009)
M. Miyamoto, H. Takeda, Earth Planet. Sci. Lett. **122**, 343 (1994)
M. Miyamoto, H. Takeda, K. Tanai, Mem. Natl. Inst. Polar Res. Spec. Issue **8**, 185 (1978)
M. Miyamoto, M.B. Duke, D.S. McKay, J. Geophys. Res. **90**, C629 (1985)
J.W. Morgan, H. Higuchi, H. Takahashi, J. Hertogen, Geochim. Cosmochim. Acta **42**, 27 (1978)
H.E. Newsom, J. Geophys. Res. **90**, C613 (1985)
H.E. Newsom, M.J. Drake, Geochim. Cosmochim. Acta **46**, 2483 (1982)
L.E. Nyquist, H. Takeda, B.M. Bansal, C.-Y. Shih, H. Wiesmann, J.L. Wooden, J. Geophys. Res. **91**, 8137 (1986)
L.E. Nyquist, H. Weismann, Y. Reese, C.-Y. Shih, L.E. Borg, Meteoritics **32**, A101 (1997)
L.E. Nyquist, Y. Reese, H. Wiesmann, C.-Y. Shih, H. Takeda, Earth Planet. Sci. Lett. **214**, 11 (2003)
L.E. Nyquist, T. Kleine, C.-Y. Shih, Y. Reese, Geochim. Cosmochim. Acta **73**, 5115 (2009)
E.J. Olsen, K. Fredriksson, S. Rajan, A. Noonan, Meteoritics **25**, 187 (1990)
C.O. O'Neill, J.S. Delaney, Meteoritics **17**, 265 (1982)
H. Palme, W. Rammensee, in *Proc. Lunar Planet. Sci. Conf.*, vol. 12B (1981), p. 949
J.J. Papike, J.M. Karner, C.K. Shearer, Am. Mineral. **88**, 469 (2003)
C.M. Pieters, R.P. Binzel, D. Bogard, T. Hiroi, D.W. Mittlefehldt, L. Nyquist, A. Rivkin, H. Takeda, Proc. IAU Symp. **229**, 273 (2005)
A. Prinzhofer, D.A. Papanastassious, G.J. Wasserburg, Geochim. Cosmochim. Acta **56**, 797 (1992)
M.N. Rao, D.H. Garrison, D.D. Bogard, G. Badhwar, A.V. Murali, J. Geophys. Res. **96**, 19321 (1991)
K. Righter, Lunar Planet. Sci. **XXXII**, CD #1765 (2001)
K. Righter, M.J. Drake, Meteorit. Planet. Sci. **32**, 929 (1997)
A. Ruzicka, G.A. Snyder, L.A. Taylor, Meteorit. Planet. Sci. **32**, 825 (1997)
R.O. Sack, W.J. Azeredo, M.E. Lipschutz, Geochim. Cosmochim. Acta **55**, 1111 (1991)
K. Saiki, H. Takeda, Meteorit. Planet. Sci. **34**, 271 (1999)
J.M. Schwartz, I.S. McCallum, Am. Mineral. **90**, 1871 (2005)
E.R.D. Scott, R.C. Greenwood, I.A. Franchi, I.S. Sanders, Geochim. Cosmochim. Acta **73**, 5835 (2009a)
E.R.D. Scott, D.D. Bogard, W.F. Bottke, G.J. Taylor, R.C. Greenwood, I.A. Franchi, K. Keil, N.A. Moskovitz, D. Nesvorny, Lunar Planet. Sci. **XL**, CD #2295 (2009b)
C.K. Shearer, G.W. Fowler, J.J. Papike, Meteorit. Planet. Sci. **32**, 877 (1997)
A. Shukolyukov, G.W. Lugmair, Earth Planet. Sci. Lett. **119**, 159 (1993)
M.I. Smoliar, Meteoritics **28**, 105 (1993)
G. Srinivasan, J.N. Goswami, N. Bhandari, Science **284**, 1348 (1999)
E. Stolper, Geochim. Cosmochim. Acta **41**, 587 (1977)
J.M. Sunshine, S.J. Bus, T.J. McCoy, T.H. Burbine, C.M. Corrigan, R.P. Binzel, Meteorit. Planet. Sci. **39**, 1343 (2004)
H. Takeda, Geochim. Cosmochim. Acta **55**, 35 (1991)
H. Takeda, Meteorit. Planet. Sci. **32**, 841 (1997)
H. Takeda, A.L. Graham, Meteoritics **26**, 129 (1991)
H. Takeda, T. Ishii, T. Arai, M. Miyamoto, Antarct. Met. Res. **10**, 401 (1997)
K. Takahashi, A. Masuda, Nature **343**, 540 (1990)
F. Tera, R.W. Carlson, N.Z. Boctor, Geochim. Cosmochim. Acta **61**, 1713 (1997)
P.C. Thomas, R.P. Binzel, M.J. Gaffey, A.D. Storrs, E.N. Wells, B.H. Zellner, Science **277**, 1492 (1997)
A.H. Treiman, Meteorit. Planet. Sci. **32**, 217 (1997)
A.H. Treiman, M.J. Drake, J. Geophys. Res. **90**, C619 (1985)
A.H. Treiman, A. Lanzirotti, D. Xirouchakis, Earth Planet. Sci. Lett. **219**, 189 (2004)
A. Trinquier, J.L. Birck, C.J. Allegre, C. Gopel, D. Ulfbeck, Geochim. Cosmochim. Acta **72**, 5146 (2008)
T. Usui, H.Y. McSween, Meteorit. Planet. Sci. **42**, 255 (2007)
H.C. Verma, V.C. Tweari, B.S. Paliwal, R.P. Tripathi, Hyperfine Interact. **186**, 181 (2008)

F. Vilas, A.L. Cochran, K.S. Jarvis, Icarus **147**, 119 (2000)
M. Wadhwa, G.W. Lugmair, Lunar Planet. Sci. **XXVI**, 1453 (1995)
M. Wadhwa, A. Shukolyukov, A.M. Davis, G.W. Lugmair, D.W. Mittlefehldt, Geochim. Cosmochim. Acta **67**, 5047 (2003)
M. Wadhwa, G. Srinivasan, R.W. Carlson, in *Meteorites and the Early Solar System II*, ed. by D.S. Lauretta, H.Y. McSween (University of Arizona Press, Tucson, 2006), p. 715
M. Wadhwa, Y. Amelin, O. Bogdanovski, A. Shukolyukov, G.W. Lugmair, P.E. Janney, Geochim. Cosmochim. Acta **73**, 5189 (2009)
P.H. Warren, Geochim. Cosmochim. Acta **49**, 577 (1985)
P.H. Warren, Meteorit. Planet. Sci. **32**, 945 (1997)
P.H. Warren, P. Gessler, Lunar Planet. Sci. **XXXII**, 1970 (2001)
P.H. Warren, E.A. Jerde, Geochim. Cosmochim. Acta **51**, 713 (1987)
P.H. Warren, E.A. Jerde, L.F. Migdisova, A.A. Yaroshevsky, in *Proc. Lunar Planet. Sci. Conf.*, vol. 20 (1990), p. 281
P.H. Warren, G.W. Kallemeyn, H. Huber, F. Ulf-Møller, W. Choe, Geochim. Cosmochim. Acta **73**, 5918 (2009)
K.C. Welten, L. Lindner, K. van der Berg, T. Loeken, P. Scherer, L. Schultz, Meteorit. Planet Sci. **32**, 891 (1997)
K.C. Welten, M.W. Caffee, A.W. Beck, Meteorit. Planet. Sci. **44**, A216 (2009)
U.H. Wiechert, A. Halliday, H. Palme, D. Rumble, Earth Planet. Sci. Lett. **221**, 373 (2004)
L.L. Wilkening, Geochim. Cosmochim. Acta **37**, 1985 (1973)
A. Yamaguchi, G.J. Taylor, K. Keil, Icarus **124**, 97 (1996)
A. Yamaguchi, G.J. Taylor, K. Keil, D.D. Bogard, Meteorit. Planet. Sci. **32**, A144 (1997)
A. Yamaguchi, G.J. Taylor, K. Keil, C. Floss, G. Crozaz, L.E. Nyquist, D.D. Bogard, D.H. Garrison, Y.D. Reese, H. Weismann, C.-Y. Shih, Geochim. Cosmochim. Acta **65**, 3577 (2001)
A. Yamaguchi, R.N. Clayton, T.K. Mayeda, M. Ebihara, Y. Oura, Y.N. Miura, H. Haramura, K. Misawa, H. Kojima, K. Nagao, Science **296**, 334 (2002)
M. Zema, M.C. Domeneghetti, G.M. Molin, V. Tazzoli, Meteorit. Planet. Sci. **32**, 855 (1997)
M.E. Zolensky, M.K. Weisberg, P.C. Buchanan, D.W. Mittlefehldt, Meteorit. Planet. Sci. **31**, 518 (1996)

Space Sci Rev (2011) 163:175–249
DOI 10.1007/s11214-011-9852-2

The Dawn Spacecraft

Valerie C. Thomas · Joseph M. Makowski · G. Mark Brown · John F. McCarthy · Dominick Bruno · J. Christopher Cardoso · W. Michael Chiville · Thomas F. Meyer · Kenneth E. Nelson · Betina E. Pavri · David A. Termohlen · Michael D. Violet · Jeffrey B. Williams

Received: 23 August 2011 / Accepted: 28 October 2011 / Published online: 3 December 2011

Abstract The Dawn spacecraft is designed to travel to and operate in orbit around the two largest main belt asteroids, Vesta and Ceres. Developed to meet a ten-year life and fully redundant, the spacecraft accommodates an ion propulsion system, including three ion engines and xenon propellant tank, utilizes large solar arrays to power the engines, carries the science instrument payload, and hosts the hardware and software required to successfully collect and transmit the scientific data back to Earth. The launch of the Dawn spacecraft in September 2007 from Cape Canaveral Air Force Station was the culmination of nearly five years of design, development, integration and testing of this unique system, one of the very few scientific spacecraft to rely on ion propulsion. The Dawn spacecraft arrived at its first destination, Vesta, in July 2011, where it will conduct science operations for twelve months before departing for Ceres.

Keywords The Orbital—JPL partnership · Early spacecraft concept evolution · Spacecraft design drivers

Acronyms

AA	Active Analog
AC	Attitude Control
ACE	Attitude Control Electronics
ACS	Attitude Control Subsystem
AMBI	Advanced Spaceborne Computer Module Bus Interface
APE	Attitude and Power Electronics
ARM	Autonomous Redundancy Management
ATLO	Assembly, Test, and Launch Operations

V.C. Thomas (✉) · G.M. Brown · B.E. Pavri
Jet Propulsion Laboratory, California Institute of Technology, Pasadena, CA 91109, USA
e-mail: valerie.c.thomas@jpl.nasa.gov

J.M. Makowski · J.F. McCarthy · D. Bruno · J.C. Cardoso · W.M. Chiville · T.F. Meyer · K.E. Nelson · D.A. Termohlen · M.D. Violet · J.B. Williams
Orbital Sciences Corporation, Dulles, VA 20166, USA